Proceedings World Geothermal Congress 2020+1
Reykjavik, Iceland, April - October 2021

1D Joint Inversion of MT and TEM Data from Ngozi Geothermal Prospect, Southwest Tanzania. An Integrated Interpretation of Geoscientific Results

Makoye Mabula Didas[1], Gylfi Pall Hersir[2]

[1]Tanzania Geothermal Development Company Limited, P. O. Box 14801, Dar es Salaam Tanzania.

[2]Iceland GeoSurvey (ÍSOR), Grensásvegur 9, 108 Reykjavík, Iceland

[1]geodidas@ymail.com, makoye.didas@tanesco.co.tz

[2]Gylfi.Pall.Hersir@isor.is

Keywords: Ngozi, Magnetotellurics, Transient Electromagnetics, 1D joint inversion, Integrated Interpretation

ABSTRACT

Ngozi geothermal prospect is the flagship prospect of the Tanzania Geothermal Development Company Limited (TGDC) located in Mbeya region within the Rungwe Volcanic Province southwest of Tanzania. The prospect is within the southern part of the East Africa rift triple junction of Rukwa, Usangu and Karonga basins where the eastern and western branches of the East African Rift System converge and form an important volcanic zone, the Rungwe volcanic Province. The thermal manifestations are mostly located northwest of the focal area. The Ngozi caldera located at an elevation of 2,620 m a.s.l forms the highest elevation of the focal area. It forms an elliptical structure with dimensions of 2.5 km long, 1.6 km wide and 74 m deep caldera forming a lake filled with chloride water on top of the mountain. Geothermometry studies of the hot springs with temperatures of 89°C, 78°C and 66°C discharging at the bottom of the lake indicated a NaCl reservoir with temperature of >230°C locally recharged by meteoric water from the Ngozi highlands, thus, making the highest temperature geothermal system so far investigated in Tanzania. This study summarizes the integrated findings of resistivity models based on 1D joint inversion of Transient Electromagnetic (TEM) and Magnetotellurics (MT) sounding data and the previous geological and structural work of the area together with geochemical results.

MT and TEM data acquired in the focal area were evaluated, reprocessed and 1D jointly inverted. The results are presented and integrated with geological and geochemical results. Based on the integrated findings from this study three drilling sites are proposed into the reservoir, which is assessed to be 4 km wide and 7 km long. The low resistivity within the fault zone at a depth between 4 and 5 km below ground level (bgl) south of Ngozi Caldera Lake is an evidence of the existence of the localized relatively young, shallow plutonic bodies which may constitute a suitable heat source for the geothermal system. The eastern and western limits of extension of the reservoir correspond to the fault zone observed in the MT cross-sections south and north of Ngozi Caldera Lake. The eastern limit of the geothermal reservoir also corresponds quite well with the fault mapped during the surface geological survey. It has been observed that the shear zones, most of the lineaments and inferred faults previously mapped in the area have remarkable displacement of the conductive anomalies in MT data.

Based on these findings, the geothermal conceptual model has been revised and the first priority zone of 28 km^2 defined as the maximum probability of hosting a geothermal system of 232°C reservoir temperature. The resource capacity of 49.4 MWe with probability P90 has been evaluated through a volumetric assessment using Monte Carlo approach.

1. INTRODUCTION

Geophysics, in particularly electrical resistivity methods, Magnetotellurics (MT) and Transient Electromagnetics (TEM) have, over the past few decades, been the most powerful geophysical tools in geothermal exploration of geothermal systems. The Magnetotelluric (MT) method is a technique for imaging the electrical conductivity structure of the Earth, from the near surface down to the a few tens of km (Chave et al., 2012). With the prevailing technology and discoveries, geothermal reservoirs located at a depth between 1 km and 4 km can be economically exploited. With geophysical methods, the physical properties of the earth's crust are examined, but a common problem is that the resolution decreases with increasing depth. Complex geological environments with 3D resistivity behaviour have often been interpreted using simple 1D models. The 1D interpretation, where it is assumed that the resistivity only varies with depth, has been successfully used for decades (Ranganayaki, 1984; Ingham and Hutton, 1982; Park and Livelybrook, 1989; Chave et al., 2012).

When investigating geothermal systems, the resistivity anomalies based on MT data can be correlated with the overall permeability distribution of the reservoir. Rocks hosting geothermal fluids usually are characterized by relatively high resistivities overlaid by an impermeable smectite-clay rich layer with anomalously low resistivity. The heat source (i.e. shallow lying hot and cooling intrusive rock or a shallow magma chamber) leaks heat by conduction mode of heat transfer into the overlying reservoir and is characterized by anomalous low resistivity. The conductive anomaly in the clay cap is attributed by the high cation exchange capacity of smectite clay minerals (Ussher et al., 2000). However, the smectite clays present in the cap rock prevents the formation of permeable open space at the top and margin of the reservoir, even where intersected by fractures (Cumming and Mackie, 2010). This clue of understanding the geometry of the conductive clay alteration is important to geothermal well targeting (Davatzes and Hickman, 2009). Therefore, the role of geophysics is to hunt the anomalies related to the geothermal system in the area.

Geophysical methods are not a standalone method. In order to constrain the geothermal system in the area, geophysical results should be integrated with geological, structural and geochemical results. These techniques help to reduce uncertainties and are the very important components for the construction of the integrated geothermal conceptual models of the area.

This report describes data processing and interpretation of the 1D jointly inverted TEM and MT data from Ngozi geothermal prospect which is located at the southern triple junction within the East African rift system in the Rungwe volcanic Province in southwest Tanzania. The report updates resistivity information previously published in Alexander et al. (2016). Also, it integrates results from geochemical studies and geological structures mapped in the area during a surface studies campaign in 2015 and 2016 (Alexander et al., 2016) and proposes three well drilling targets. Moreover, based on the integrated results the resource is estimated using the Monte Carlo volumetric assessment.

2. GEOLOGICAL AND GEOTHERMAL CONDITIONS IN TANZANIA AND THE NGOZI AREA

2.1 Geological and Regional Tectonic Setting of Tanzania

The African continent is gradually splitting apart along the East African Rift valley, a 3,000 km long series of deep basins and flanking mountain ranges (Figure 1). The East African Rift System (EARS) starts from the Afar region in Southeast Eritrea and North Ethiopia (Figure 1) forming the Afar triple junction. The rift stretches all the way south through Ethiopia, Kenya and North Tanzania where it splits into two branches, the Eastern and the Western Rift (Figure 1). The two branches extend further south. In Tanzania, the two branches of the EARS converge at Mbeya area forming a triple junction within the Rungwe Volcanic Province (Delvaux and Hanon, 1993) before extending further south to Malawi and Zambia where is terminated. The EARS being a continental-continental spreading plate boundary is a potential area for geothermal resources in East Africa. Here, the continent is stretched, thinned and heated to the point of breaking. Hot, partially melted rocks rising up from the upper mantle are either erupting at the Earth's surface or cooling within the crust. This is an important phenomenon which provides elevated heat sources for the geothermal systems. So far, Kenya is the only country in the Rift system that has taken use of geothermal resource over 600 MWe produced in Olkaria field. No potential geothermal resource has been discovered within the western branch but high temperature surface geothermal manifestations are prominent (see Figure 2) and more efforts are underway to discover and exploit geothermal resource for electric power generation and direct use. Apart from the volcanic hosted geothermal system which is along the EARS, several low-medium (fault controlled) geothermal systems can be found in older rocks (Precambrian rocks and in Mesozoic sedimentary basins) in Tanzania (Figure 2).

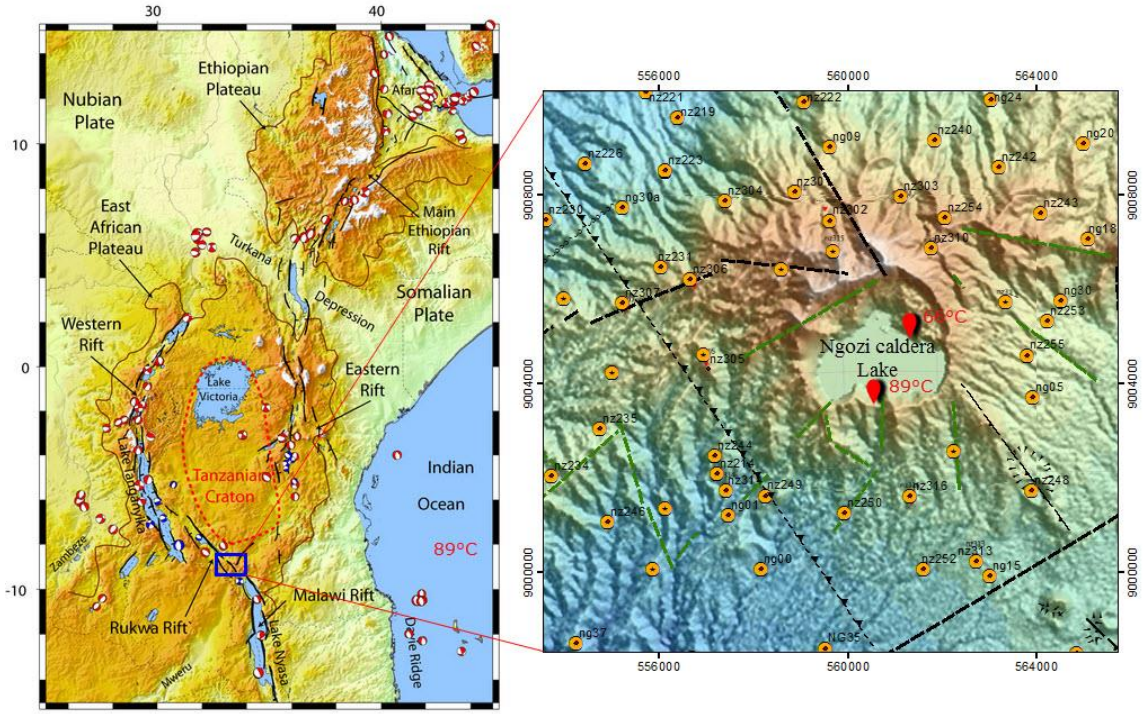

Figure 1: The East African Rift System: the red and white filled circles indicate the focal mechanisms for earthquakes in the area (EARS, 2018). The blue box is the Ngozi prospect zoomed in the right. Yellow circles are MT-TEM stations.

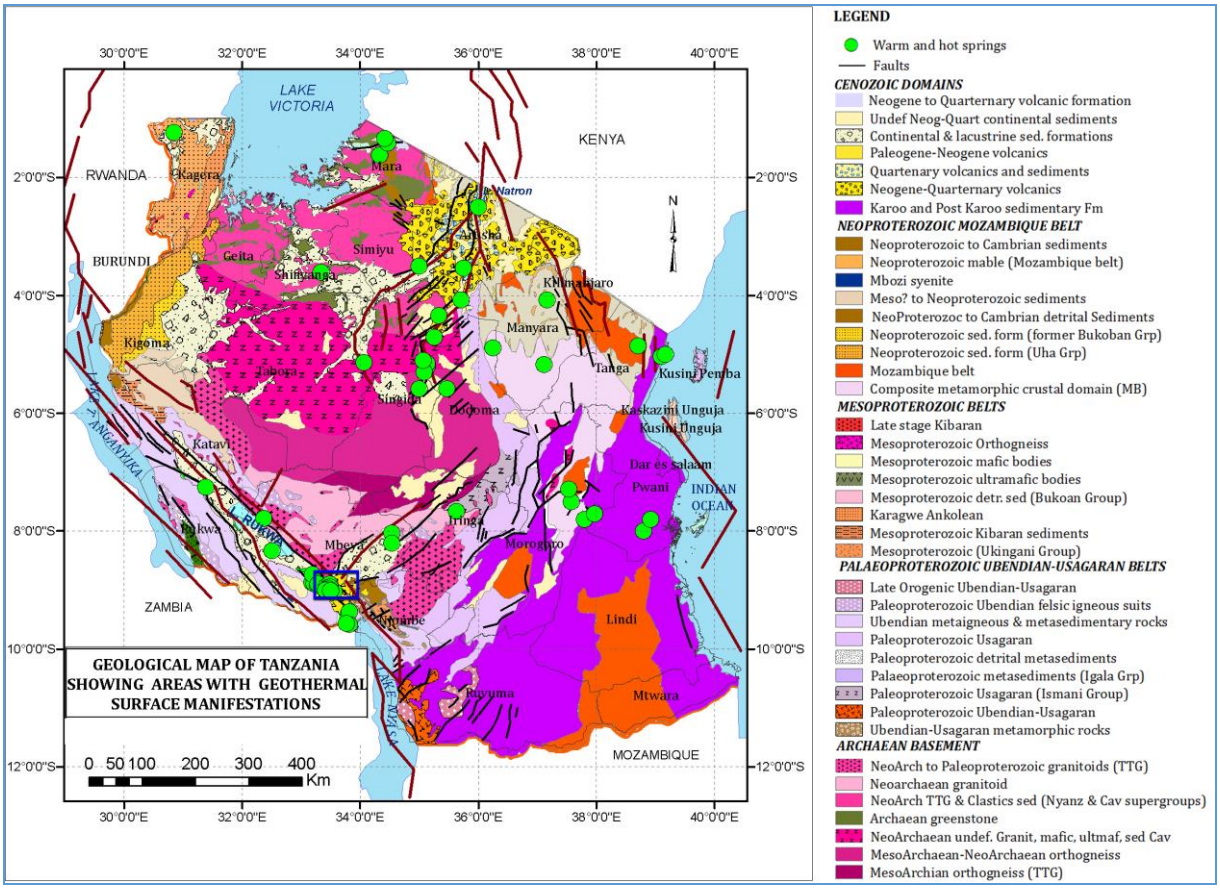

Figure 2: Geological map of Tanzania showing the location of Ngozi Geothermal prospect (boxed in blue) at the triple junction of the EARS (red lines). The green circles are the surface geothermal manifestations. Map modified from Pinna et al. (2008).

2.3 The Ngozi Geothermal Prospect

2.3.1 Location of the study area

Ngozi geothermal area is located about 10 km southeast of Mbeya Town on the southern triple junction axis of the EARS within the Rungwe volcanic Province (see Figure 1 and 2) which consists of main four volcanic eruption centers: Ngozi (2,620 m a.s.l), Rungwe (3,000 m a.s.l), Tukuyu (1,300 m a.s.l) and Kiejo (2,200 m a.s.l). The triple junction consists of three major rift basins, the Rukwa-Tanganyika Basin trending northwest (in the north), the less developed Ruaha-Mtera-Usangu depression trending NE (in the east) and the Karonga basin (Malawi rift) trending southeast which stretches to the south through Malawi and culminated in Zambia.

2.3.2 Geological and Geothermal setting of Ngozi prospect

Ngozi volcanic center is an uplifted (more than 2,500 m a.s.l), elliptical structure forming a 2.5 km long, 1.6 km wide, and 74 m deep caldera filled with water on top of the mountain (Josephat, 2016). This Crater Lake is classified as the second largest in the East African Rift and in Africa (Delalande et al., 2015). It was formed in Late Quaternary to Holocene (Fontijn et al., 2010a; Fontijn et al., 2012; Delalande et al., 2015) during an uplift caused by shallow intrusions of rhyolitic magma which episodically erupted depositing large volumes of volcanic pumice, scoria and other forms of pyroclastic. This was accompanied by a series of small eruptive centres observed in the area as volcanic cones, domes and eruption craters resulted from the continental hotspots or plume activity (Ebinger et al., 1989; Delalande et al., 2015). The Ngozi volcanic system comprises the Ngozi dome as the central volcano with a collapsed structure at its central forming a caldera filled with a mixture of magmatic (30-35%) and meteoric (70-65%) waters (Kraml et al., 2008; Alexander et al., 2016). A 4 km wide NW-SE trending fault zone whose eastern arm is partly mapped on surface data transects the Ngozi dome. Three hot springs connected by the N-S structures with temperature of 89°C, 78°C and 66°C were mapped at the bottom of the lake (Kraml et al., 2008).

Generally, Ngozi and its surrounding areas are covered with varieties of rock types. Quaternary ash pumice resulting from Ignimbrite volcanic eruption within the last 1 Ka (Fontijn et al., 2010b) covers an extensive area (Figure 3). Alluvial sediments deposited in depocentres on top of the basement or older volcanics, cover the low plains of Ngozi and are overlain by the Quaternary ash pumice. The alluvial sediments disappear close to the dome area. It is likely that the surface had been uplifted, exposed and eroded during the dome stage about 10 Ka or/and completely removed from deeper surface during an episodic eruption phase up to 1 Ka in the dome area and the spaces were occupied by the young volcanic rocks.

Ngozi prospect is characterized by three main sets of faulting trends; the NW-SE major trend, the NNE-SSW trend and the NE-SW structural trends most of them mapped from remote sensing (Alexander et al., 2016). The NE and NW faults follow the current stress regime and are therefore interpreted to be young faults, reactivated due to stresses at the triple junction (Fontijn et al., 2010a).

The NW trending inferred fault which connects several eruption centers northwest and southeast of the Ngozi caldera and passes through the Lake has been observed in this study to be about 4 km wide towards west forming a graben structure of about 7 km long engulfing the Ngozi caldera lake. This fault zone was interpreted by Fontijn et al. (2012) as a narrow NW-SE buried rift fault dextral truncated by the NE –SW trending faults southeast of the Ngozi caldera.

The geochemical studies conducted so far, consider the Ngozi area to be a high temperature geothermal field based on data from three hot springs. Three hot springs with temperature of 89°C, 78°C and 66°C were mapped at the bottom of the Ngozi Crater Lake (Kraml et al., 2008). The hot springs were of NaCl composition. Na-K geothermometry from the three hot springs in the Lake (66-89°C) indicated reservoir temperature of >230°C locally recharged by meteoric water from the Ngozi highlands through fractures, faults and possibly fissures (Ochmann and Garofalo, 2013). This observation is the most important geochemical evidence of the existence of a high temperature geothermal system in the area.

Several hot springs of temperature ranging between 30°C and 84°C are located northwest and southwest of the area and have different geochemical composition (Na-HCO_3) and properties. It has been concluded that they are heated water through conduction, discharging from the deep-seated faults with reservoir temperature ranging from 120°C to 130°C (Josephat, 2016; Alexander et al., 2016). Petrographic study of rock samples using XRD analysis indicate different clay minerals including kaolin, illite, smectite and other secondary minerals like calcite, quartz, epidote and zeolite. The presence of quartz, illite and epidote mineral assemblage indicates that the rocks were once exposed in the geothermal reservoir environment (Alexander et al., 2016).

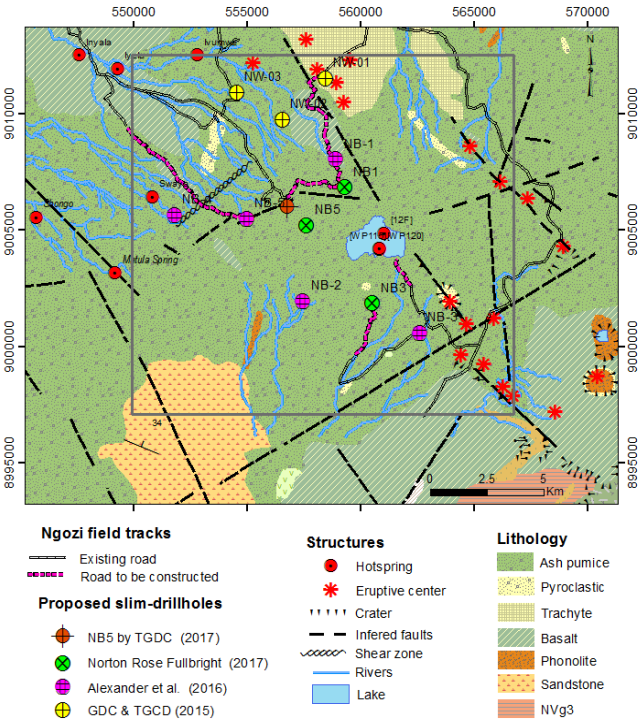

Figure 3: Geological map of the Ngozi geothermal prospect with tectonic structures and surface geothermal manifestation. Map modified from Alexander et al. (2016). The grey box is the study area.

2.4 Previous Geothermal Studies in Ngozi (General Review)

Geothermal exploration studies in Ngozi prospect date back from 2006 to 2013 within the framework of GEOTHERMAL technical corporation programme implemented by the Federal Institute of Geosciences and Natural Resources (BGR, Hanover, Germany), on behalf of the Federal Ministry for Economic cooperation and development and the government of Tanzania (Kraml et al., 2008; Kalberkamp et al., 2010; Ochmann and Garofalo, 2013). Earlier, there had been several academic based research studies in the area (e.g. Ebinger et al., 1989; Delvaux et al., 1992; Ebinger et al., 1993; Delvaux and Hanon, 1993; Delvaux et al., 1998; Gibert et al., 2002) mostly focusing on the regional tectonic and volcanological evolution of the Western branch of the East African Rift System and volcanism of the Rungwe volcanic Province at the triple junction. Major geothermal findings were first revealed during the GEOTHERMAL technical corporation programme (Kraml et al., 2008). The results included the first mapping of the three hot springs with temperature 89°C, 76°C and 66°C located at the bottom of the Ngozi caldera lake. The geochemical study concluded that the NaCl rich hot springs were discharging from the geothermal reservoir with a temperature of 232°C (based on Na-K geothermometry) located below the Ngozi caldera lake. However, the major conclusion from the study was that, Ngozi and Songwe were a single geothermal system, Songwe being the outflow from Ngozi which was regarded to be the up flow.

Based on surface geological studies in 2006 to 2010, Delvaux et al. (2010) concluded that the Ngozi geothermal system was located between the Ngozi caldera and the Mbeya town. They suggested that the discharge area is in Songwe valley and the system is recharged from the Ngozi volcano area influenced by the strong latitude gradient. This meant that the proposed geothermal reservoir was located far northwest of the Ngozi caldera. Similar interpretation was done by Kraml et al. (2008) and Kalberkamp et al. (2010) based on the interpretation of a magnetic low from the regional aeromagnetic survey in Marobhe (1989).

These important conclusions were rejected by Alexander et al. (2016) during the integrated detailed surface geological and structural mapping, geochemical studies (soil gas sampling, fluid gas sampling, and water chemistry from the hot/cold springs from rivers and shallow drill boreholes), ground magnetic and gravity surveys as well as co-located MT/TEM soundings. Based on their results, Alexander et al. (2016) concluded that Songwe and Ngozi are two different geothermal systems; Ngozi being a high temperature volcanic hosted geothermal system with reservoir temperature of 232°C and Songwe was being a low-medium temperature fault controlled geothermal system. The study also concluded that the hot springs at the bottom of the lake were discharging from the 232°C hot reservoir located below the Ngozi caldera. The shallow trachytic intrusive below the caldera was regarded as a potential heat source of the system. The chemical composition of the Ngozi hot springs and the lake water was NaCl while the warm and hot springs located west-northwest and in Songwe prospect were all $NaHCO_3$. However, it was reported that most of the MT soundings at great depth had strong 3D effect. In the inversion, a 1D earth model was assumed. Therefore, in order to minimize the 3D effect, the low frequency part of the data (reflecting depths greater than 2 km) were chopped off and never used. This had a great effect as information on resistivity at great depth was missing. Neither faults, nor heat source could be mapped at these shallow depths from the MT soundings. Moreover, the correlation between the geological structures and resistivity anomalies were missing in the report by Alexander et al., (2016). The integrated conceptual model concluded that the geothermal system in Ngozi is constrained below the caldera itself, but it may extend laterally to the west to a maximum distance of 2,500 m from the Ngozi caldera rim with 10% level of confidence (Alexander et al., 2016). Finally, Alexander et al. (2016), propose four slim well drilling targets, all of them are located outside of the optimum resource boundaries because using a conventional drilling rig the area would not be accessible.

In 2017, the Government of Tanzania through the Ministry of Mineral and Energy and Tanzania Geothermal Development Company Limited (TGDC) contracted Norton Rose Fulbright consulting company to assess the potential geothermal resources in the top five best prospects in Tanzania including Ngozi (Norton Rose Fulbright, 2017). They recommended that the drilling targets proposed by Alexander et al. (2016) should be shifted closer to Ngozi caldera. TGDC sent a field crew to Ngozi and observed that two wells (NB1 and NB5) out of the three could be shifted. Therefore, it was decided to reprocess and 1D invert the MT-TEM sounding data in this project and integrate the resulting resistivity model with the geochemical and surface geological data.

3. METHODOLOGY

3.1 Surface Geological Mapping

The geological method used in this study was the detailed lithological and structural mapping (fault, fractures, dykes, alteration minerals, volcanology, volcanic history, hydrogeology etc.) done in Ngozi geothermal prospect by Alexander et al. 2016. It was performed in order to obtain some information based on surface geological information about the surface features of the area. For example, what temperature is to be expected, how big is the geothermal field, where to drill (high temperature and permeable fractures or formation in the reservoir)? It is an important tool for mapping surface distribution of the lithology (rock types) of the area, the alteration and the surface manifestations, and suggest a possible heat source. Moreover, it was used to identify the structures e.g., fractures, joints and faults that may be the important conduits for the fluid migrations. This method is limited to surface observation. Hence, it does not give the detail subsurface information of the area. Thus, in this study the geological findings have been integrated with the geophysical findings from MT and TEM surveys and interpreted all together.

Outcome: Three possible outcomes were generated from the geological studies including maps and cross-section, a preliminary conceptual model (showing the possible upflow/outflow zones, depth to the heat source) and a report. However, the geological method is limited to direct observations on surface and does not probe deep into the earth's crust.

3.2 Geochemical Method

To infer the reservoir geochemical conditions in the area samples from the hotspring springs were analysed by Alexander et al. 2016. Among the work done included the investigation of the subsurface composition of the reservoir fluids, estimate the fluid temperature of the reservoir and evaluate subsurface processes within the reservoir such as boiling or mixing. This was done by sampling and analysing the geothermal fluids (which is present in form of hotsprings) of the reservoir that have been discharged to the surface through faults and fractures. The analytical results from the fluid samples (water and gas samples) has been used to predict the temperature of the reservoir (through chemical geothermometry studies), equilibrium state, and salinity, gas content of the reservoir fluid, recharge/origin of fluid and flow directions (through isotopic studies) of the fluid (Alexander et al. 2016 and Josephat 2016). The geochemical results have been integrated with the geological and the geophysical results to generate a conceptual model.

3.3 Magnetotelluric (MT) Method

The magnetotelluric method is a natural source electromagnetic method using frequency from several hundreds of Hz to less than 0.001 Hz. It can probe the Earth and measure electrical resistivity to depths of several tens to hundreds of kilometers (Chave et al., 2012). It is this capability of penetrating deep into the subsurface Earth that has made it to be the only method for studying deep resistivity structures (Jones, 2008). In MT survey the fluctuations in the natural electric field, **E** and magnetic field, **B**, which are measured in orthogonal directions at the surface that allows us to determine the electrical resistivity distribution of the Earth at depth. In MT survey, Low frequencies (<1 Hz) are generated by ionosphere and magnetosphere currents caused by the solar wind (plasma) emitted from the sun and interfering with the Earth's magnetic field (Figure 5). The high frequencies (>1 Hz) are generated by the lightening discharges from the equatorial regions and propagates around the world within a waveguide bounded by the ionosphere and the Earth's surface (Chave et al., 2012).

3.3.1 Instrumentation and data acquisition

The Magnetotelluric data set include, 64 soundings collected from three survey campaigns. The first survey was done by the BGR in 2008 -2013 (MBY* stations), followed by TGDC and GDC (ng* stations) in 2015 and TGDC in 2016 (nz* stations). The

locations of the soundings are shown in Figure 1 and 16. MT soundings by BGR were acquired using Metronix MT unit while the rest MT soundings done by TGDC and GDC were acquired using 5-channel MTU-5A receiver using MTC-50H magnetic coils.

3.3.2 Data processing (time series analysis)

MT data were processed using a combination of different approaches described in Phoenix MT processing manual (Phoenix, 2005) in the following workflow:

i. Viewing the time series data using Synchro Time series view program in SSMT2000 software. This program allows graphical viewing of the time series and has an option of printing the computed power spectra density and coherence between pairs of orthogonal channels.

ii. Decimation of the time series data as described by Wight et al. (1977) and Wight and Bostick (1980) through visual inspection so as to recognize and exclude noisy data from the records.

iii. The conversion of the decimated time series data into frequency domain using Fast Fourier Transformation method (Bendat and Piersol, 1971) in SSMT2000 program. This produced the Fourier coefficients (parameter) which were then used to calculate high and low frequency MT plot files (MTH, MTL) with multiple cross powers for every frequency.

3.3.3 Data processing - edi file format

The computed high and low frequency MT files (MTH, MTL) from SSMT2000 were used as input files in the MTEditor software. In MTEditor the resistivity and phase for every frequency were edited. The editing is either done automatically or manually. The edited files were saved as .mpk files and finally exported to an industry standard edi file (electronic data interchange) suitable for use with other geophysical inversion software like TEMTD or WinGLink where joint inversion with TEM data is performed.

3.3.4 Choosing a resistivity invariant

In 1D inversion of MT data, several invariants exist, and the question arises which apparent resistivity curve to invert for. This is discussed by Park and Livelybrooks (1989). Three types of average, determinant, arithmetic average and the geometric mean were computed (Figure 4) and compared as described in Park and Livelybrooks (1989). The arithmetic mean had a big sense results to the other invariants and thus was used as the reasonable and stable mean for the inversion. The arithmetic mean invariant parameter was chosen over the determinant and the geometric mean because it yielded stable and reasonable estimates of the rhoxy and rhoyx resistivities in each MT data station see Figure 4 and Appendix 1 in Didas (2018). According to Park and Livelybrooks (1989); for a 1D earth response the determinant (det), the geometric mean (gme) and the arithmetic mean (ave) gave the same value. For 2D earth, the det, and gme were reduced to the same value but the ave was different. For 3D earth, all these parameters were different. Based on Park and Livelybrooks (1989) descriptions it was observed that most of the stations used in this study at shallow depths (high frequency) are 1D but at relatively greater depths have either 2D or 3D effects. However, there were few stations which were 1D throughout the frequency range of investigation. The determinant invariant which has been commonly used in MT inversion at ISOR as suggested by Park and Livelybrooks (1989) in this case it doesn't work for the Ngozi MT data presented in this study.

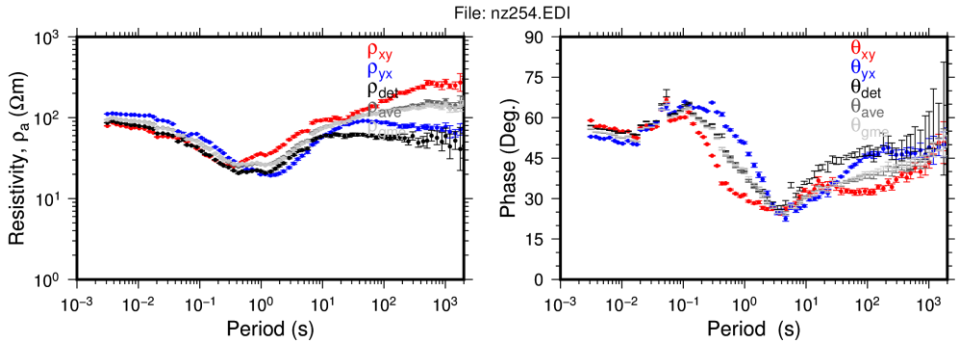

Figure 4: Processed data for MT sounding nz254 - apparent resistivity and phase curves for different parameters. All the invariant parameters were different. Note how the determinant visually matches "a local 1D resistivity model" but deviates at this site for periods above 10 s.

3.4 Transient Electromagnetics (TEM) Method

The Transient Electromagnetics, TEM method (also known as Time Domain Electromagnetics, TDEM), is a geophysical exploration technique which detects subsurface electrical resistivity properties from a few meters below the surface to several hundreds of meters depth (see Árnason, 1989 and references there in for detailed mathematical expression**)**. The depth of penetration in TEM surveys depends on the subsurface resistivity, current induced, receiver sensitivity, and transmitter-receiver geometry (size of the transmitter loop). In TEM, electric and magnetic fields are induced by transient (short time varying) pulses of an electric current in a loop or dipole and the subsequent decay response is measured. Unlike the MT method, TEM is an active method wherein the primary magnetic field is known. The decay response measured in the TEM receiver is the magnetic field created by the eddy currents in the subsurface. The TEM survey was performed to estimate the static shift affecting MT data collected at the same MT locations.

3.4.1 Instrumentation and data acquisition

In this study, 64 TEM soundings were collected by using Zonge GDP32[24] TEM equipment using a 100 m x 100 m square transmitter loop and a central receiver, measuring the vertical component of the magnetic field. The data were processed and jointly inverted with MT data to generate a 1D Occam model. Like for the MT data, the TEM data used in the inversion were collected from three survey campaign by the BGR in 2008 -2013 (MBY* stations), TGDC and GDC (ng* stations) in 2015 and TGDC in 2016 (nz* stations). The location of the soundings is shown in Figure 1 and 7. TEM soundings by BGR were acquired using Geonix-7 receiver. The rest of the soundings were acquired using Zonge GDP32[24] TEM equipment.

3.4.2 TEM data processing (raw data analysis) using TemX program

Prior to modelling, the raw TEM data were converted to suitable file format *.USF files by using several software made available by the instrument manufacturer. The *.CAC files produced by the Zonge receiver were converted to *.AVG format by the 'TEMAVGW" program and then to *.USF format by the "TEMTRIM" program. The *.USF files are the input files for the TemX program made at ISOR (Árnason, 2006a). The TemX program reads and processes the standard file formats of the central loop TEM data. It performs normalization of the voltages with respect to the transmitted current, gain and effective area of the antenna and then displays all the data graphically, allowing the user to omit outliers, calculates averages over data set and calculates the time apparent resistivity. The program produces an output file *.inv ready for inversion in inversion programs such as TEMTD explained in the following chapter.

4. 1D JOINT INVERSION OF MT AND TEM DATA

The 1D TEM-MT joint inversion in this study was done by TEMTD software. TEMTD is a 1D inversion program where a horizontally layered earth model for central square-loop TEM and MT data is used. The program was developed at ISOR in 2006 (Árnason, 2006). It can also be used to invert separately TEM or MT data. The TEMTD software is written in ANSI-C and runs under UNIX/LINUX operating systems and uses the gnuplot graphics programme for graphical display during the inversion process. The program can be used to perform both layered inversion and minimum structure (Occam) inversion of which the fixed thickness of the layers increases exponentially with depth. In this study Occam inversion was used.

For the initial/starting model for the inversion, the first layer was assigned a fixed thickness of 10 m and the half-space was given a constant resistivity value between 10 Ωm and 30 Ωm. For most of the inversions an initial model with 50 layers was used. Damping factors were applied to smooth the output model. The misfit of the model was evaluated by the chi-square factor. The highest chi-square error in the final fit was 11.6 most errors were less than 2 (see Appendix 2 in Didas, 2018). The inversion was done through jointly inverting the TEM data and the rotationally invariant apparent resistivity and phase of MT calculated from the average (arithmetic mean) of the off-diagonal impendence tensor elements. To estimate the static shift affecting MT data, we used TEM data collected at the same (or with a maximum of 100 m offset) MT locations. Following the approach proposed by Meju (1996), the MT and TEM data (both not affected by the static shift) have been jointly inverted to retrieve a 1D undistorted resistivity model at each site as shown in in Figure 5.

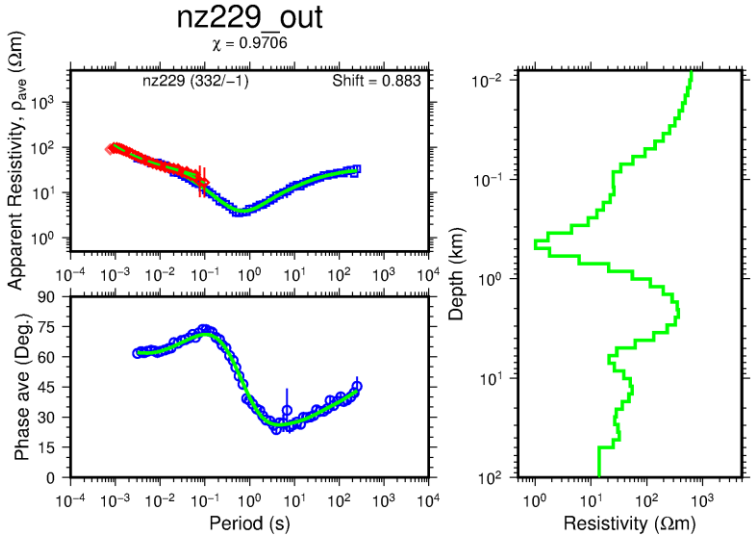

Figure 5: Example of the result of joint 1D Occam inversion of TEM and MT data. Red diamonds are measured TEM apparent resistivities, blue squares are measured MT apparent resistivities, and blue circles are the MT phase. The green curve to the right shows the resistivity Occam model vs. depth. The calculated response of the resistivity model is given by the solid green lines in the two panels to the left. The shift multiplier is shown in the upper right hand corner of the apparent resistivity panel. The 322 m in the parenthes (x/y) is due to difference in coordinate projections between colocated MT (in WGS84) and TEM (in ARC1960) stations.

4.1 Static Shift Multiplier of MT Data in Ngozi Prospect

In the Ngozi prospect, the static shift multiplier for each MT sounding was calculated using the arithmetic mean invariant values for the apparent resistivity through joint inversion with data from collocated or nearby TEM sounding. The multipliers were in the range of 0.1 to 4.7, most commonly around 0.6 (Figure 15). In the static shift correction of MT data, the apparent resistivity values

are divided by the shift multiplier. The spatial distribution of the multipliers is shown in Figure 6. From the histogram (Figure 6) we can see that the majority of the soundings were shifted up (shift factor <1) and only a few shifted down (shift factor >1). The highest static shift factor is observed southwest and northwest of the Ngozi caldera where shallow-subsurface alluvial sediments are found. The low static shift factors are observed around the dome area at high topography: this indicates that Steep slopes in the area are have strong distortion effects on the telluric currents.

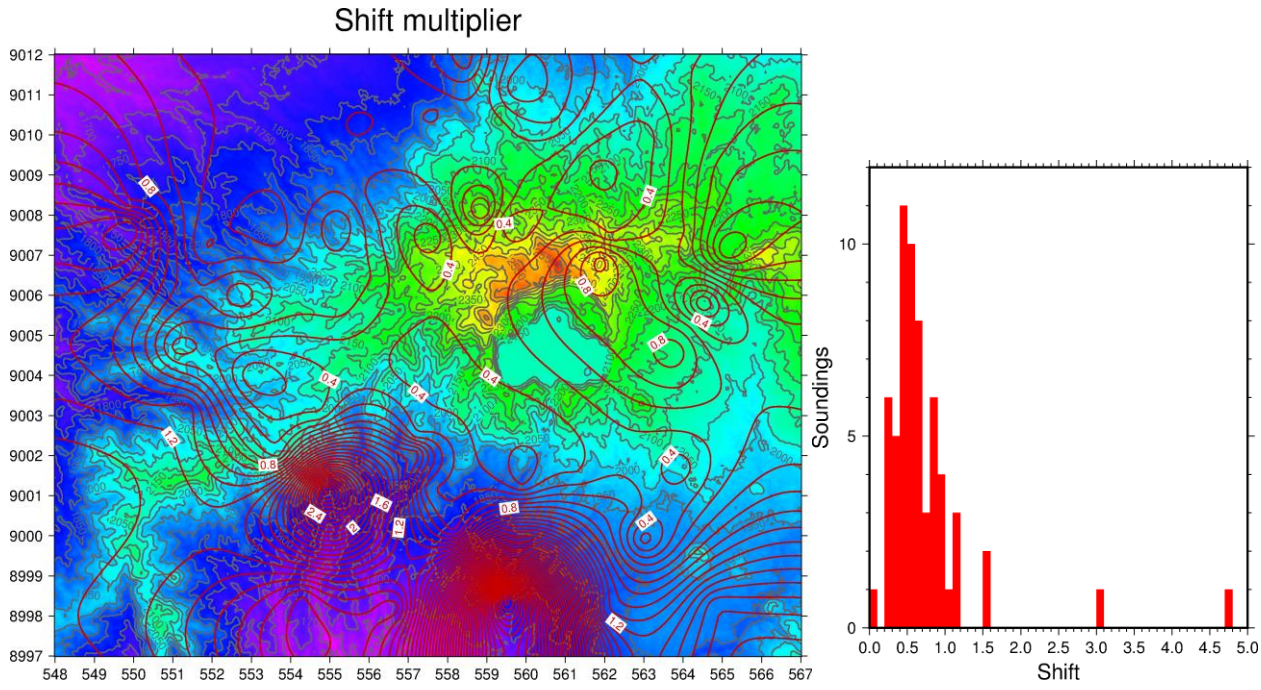

Figure 6: a) Spatial distribution of static shift multipliers. b) Histogram distribution of static shift multipliers in Ngozi prospect in the Ngozi prospect.

5. RESULTS

The result of 1D Occam inversion of 64 co-located MT/TEM sounding pairs, using the arithmetic mean invariant values for the MT apparent resistivity and phase, are presented here as vertical resistivity cross sections and as resistivity maps at different elevations (depth slices). However, we interpreted our results with some degree of uncertainty due to 1D models could possibly have high error at greater depth.

5.1 Resistivity Cross Sections

The resistivity cross-sections in this study were generated using the TEMCROSS program (Eysteinsson, 1998). For clarity here we present only four cross-sections but more cross-sections the reader is referred to Didas (2018). They show resistivity structures to 5 km depth below sea level. Their locations are displayed in Figure 7 and five of them are discussed in this report to emphasize the main results of the 1D inversion. For clarity of dimensionality of the data the results are presented using strike and induction arrow analysis.

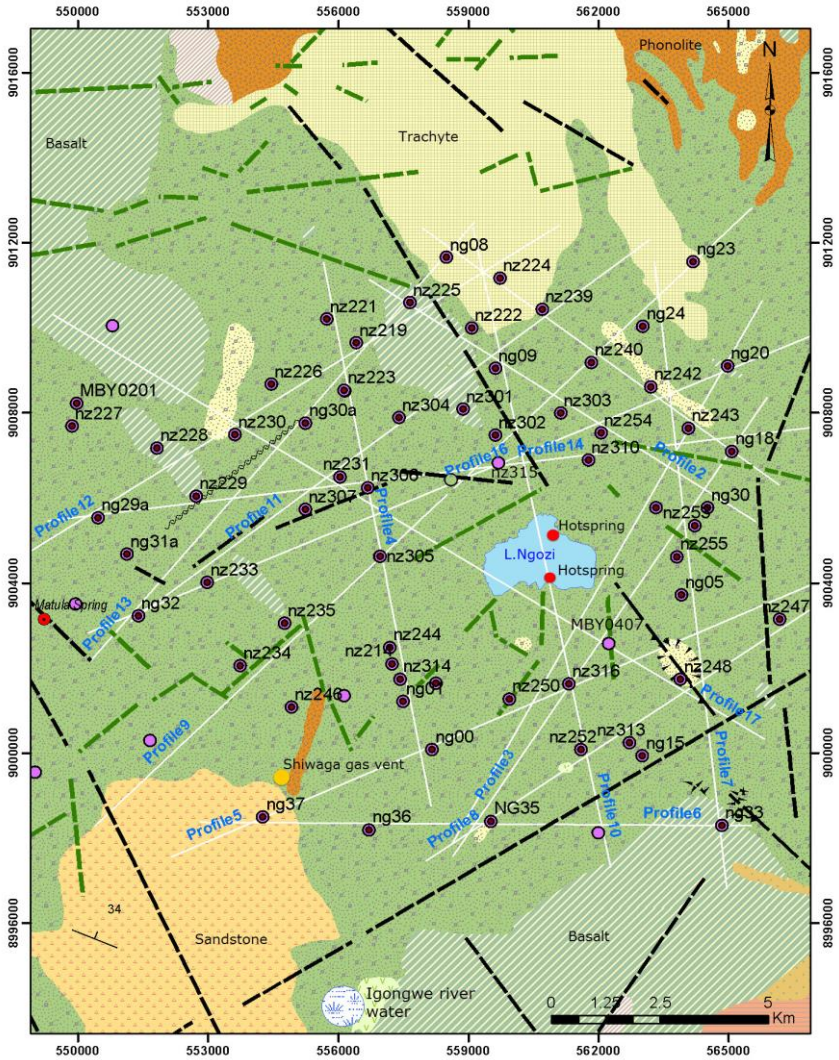

Figure 7: Location of the resistivity cross-sections (white lines superimposed on the Ngozi geological map). The black stipples lines are the inferred faults mapped on surface and green lines are lineaments extracted from Shuttle Radar Topogrphic Mission 90 m resolution Digital Elevation Model. The black doted circles are the MT/TEM sounding pairs and MT stations without TEM are circles without dotes.

5.1.1 Resistivity cross-section along profile 5

The cross-section in Figure 8 is located about 2,400 m south of the Ngozi caldera lake. It trends from SW to NE and crosses the southwest dipping NW trending inferred thrust fault mapped by Alexander et al. (2016) at MT station nz248. The main visible features are:

i. A resistive surficial zone of 100 -200 Ωm and maximum thickness of about 200 m.

ii. A well-defined conductive cap of 1-10 Ωm with thickness of about 500 m, centred at a depth of about 1,400 m a.s.l and surrounded by a 10-30 Ωm conductive layer with thickness of up to 1 km.

iii. A moderately resistive zone of 30-70 Ωm below the conductive layer with thickness of about 1,500 m centred at sea level.

iv. A vertical conductive anomaly of 10-30 Ωm, 5 km wide with some very conductive < 10 Ωm patches below the moderately resistive zone imaged by MT stations ng00 and nz316.

v. A resistive zone of 70-100 Ωm to the east of the vertical conductive anomaly.

vi. A very resistive zone 100-200 Ωm to the west of the vertical conductive anomaly. The top surface is defined by 100 Ωm iso-resistivity line below the Shiwaga CO2 gas vent down to a depth of about 1,000 m.

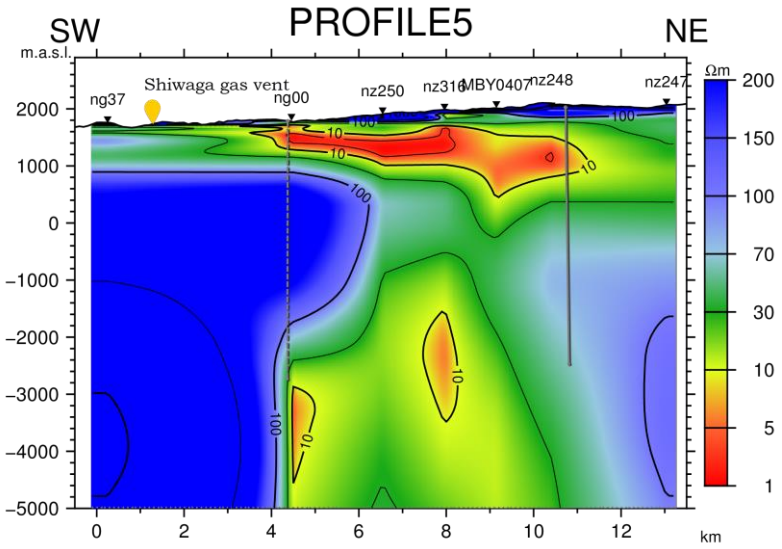

Figure 8: Resistivity cross-section along profile 5 (location on Figure 7).The grey straight line is the projection of the inferred fault mapped onthe surface and the dotted line represents the western end of the same fault.

5.1.2 Resistivity cross-section along Profile 9

Profile 9 is located 1,800 m northwest of Ngozi caldera (see Figure 7). The cross-section was generated with the purpose of observing extension of the fault zone revealed on profile 5 which is located about 2,400 km south of the Ngozi caldera. The main observations are:

i. The surficial resistive layer with resistivity > 100 Ωm thickening up to 500 m over the Ngozi caldera rim and thinning away towards SW and NE respectively.

ii. A 10-50 Ωm zone with some < 10 Ωm anomaly patches. It is thickening within the fault zone between MT station nz305 and nz302 relative to the adjacent <10 Ωm resistivity anomaly in the SW.

iii. A well-defined 100 Ωm anomaly about 400 m thick below MT stations nz303, nz240 and ng24 below the resistive thinned surficial layer.

iv. The >100 Ωm resistive zone which is very extensive below the conductive anomalies. It is from a depth of 1,200 m a.s.l. The top part of this anomaly is defined by the 100 Ωm resistivity iso-line.

v. A <100 Ωm resistivity anomaly imaged by MT stations nz234 and nz235 at a depth of about 1,500 b.s.l.

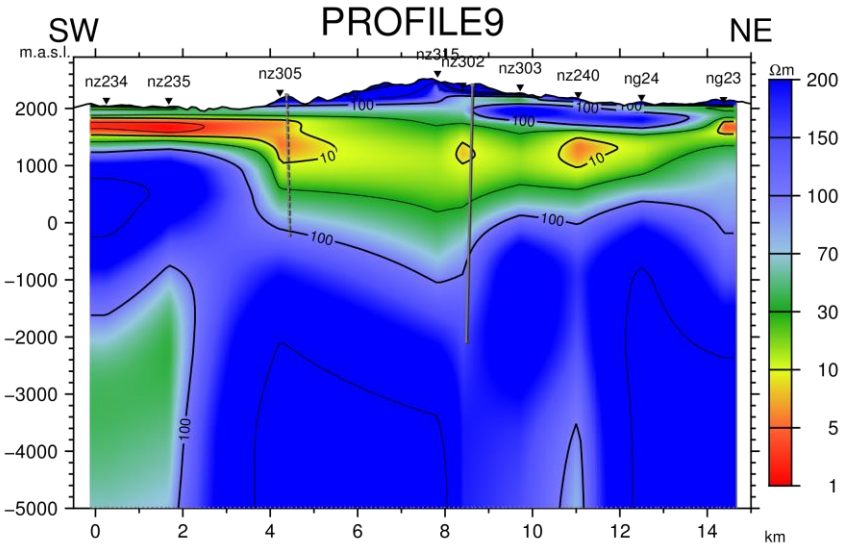

Figure 9: Resistivity cross-section along profile 9 (location on Figure 7). Grey straight line is the projection of the inferred fault mapped on surface and the dotted line represents the western end of the same fault.

5.1.3 Resistivity cross-section along Profile 10

Profile 10 passes through the Ngozi hot springs (located at the bottom of the lake) and crosses the NW-SE trending inferred fault at MT station nz302 (see Figure 7). The cross-section along this profile primarily was generated with the purpose of mapping the southwest and northeast extension of the fault zone mapped north and south of the caldera along profile 5 and 9, respectively. The second purpose was to investigate vertical conductive anomaly observed in cross section 5 across the Ngozi caldera lake. Station nz316 is about 2,700 m to the south of the hot springs and station nz315 is about 1,600 m north of the lake. Unfortunately, there are MT sounding gap between nz316 and nz315. The main visible features are:

i. The resistive surficial zone with resistivity >100 Ωm thickening towards the rims of Ngozi caldera lake and thinning away each side.

ii. The conductive layer < 10 Ωm, relatively horizontal to the SSE and NNW, respectively, terminates before reaching the Ngozi caldera. The conductive anomaly on top of the vertical anomaly from nz252 to nz316 as it approaches the fault boundary SSE of the Ngozi hot spring is relatively elevated (up domed). However, there is no evidence to support this observation due to lack of MT data close to the caldera.

iii. A vertical moderate conductive zone > 10-30 Ωm below MT station nz316 associated with a 10 Ωm patch.

iv. Two very extensive resistive zones of > 100 Ωm below the conductive anomalies and separated by a vertical moderate conductive anomaly. It is located from around sea level in the NNW part and deepens towards SSE at 1,000 m b.s.l. The top part of this anomaly is defined by the 100 Ωm iso-resistivity line.

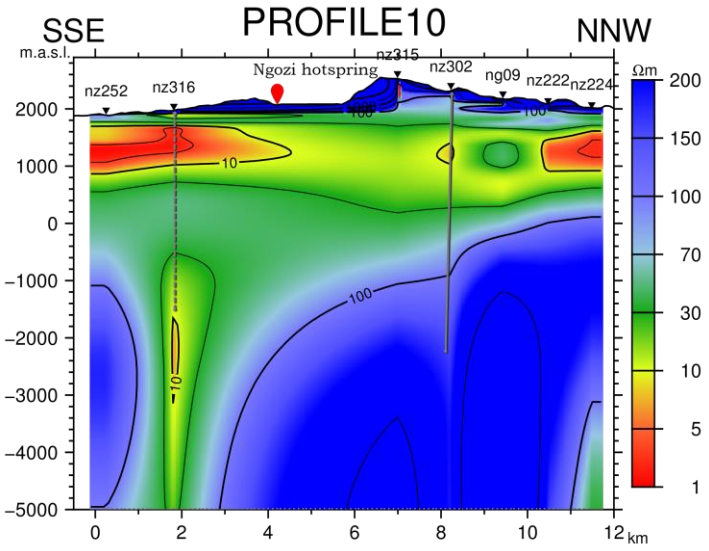

Figure 10: Resistivity cross-section along profile 10 (location on Figure 7). Grey straight line is the projection of the inferred fault mapped on surface and the doted line represents the south extension of the same fault.

5.1.4 Resistivity cross-section along Profile 11

Profile 11 is located about 3,700 m northwest of Ngozi Caldera Lake and about 1,900 m away from profile 9 (see Figure 7). The resistivity cross-section along Profile 11 (Figure 11) was generated with the objective of investigating the northern extension of the fault zone mapped in cross-section 9. The main visible features are:

i. The resistive > 100 Ωm surficial layer thickening to about 600 m at the center of the cross-section and thinning away to both sides.

ii. A conductive layer < 10 Ωm of about 200 m thickness SW of the cross-section and thickening to about 800 m NE of the cross-section. The NE anomaly is enclosed by the 10-50 Ωm resistive anomaly. It is displaced downwards between MT station nz307 and nz231 to a depth of about 1,000 m by the inferred fault mapped on surface represented by a grey dashed vertical line (Figure 7).

iii. A 10-50 Ωm resistivity layer located below the conductive layer < 10 Ωm in the SW and overlain by the resistive surficial layer from the central part of the profile towards the NE. It is thick up to 2 km within the fault zone and is elevated in SW.

iv. Vertical anomaly with resistivity between 70 and 100 Ωm within the fault zone.

v. A resistive > 100 Ωm extensive zone overlain by the 10 -50 Ωm layer and separated by a vertical resistivity anomaly. Similarly, the top part of the >100 Ωm anomaly is defined by 100 Ωm iso-resistivity line.

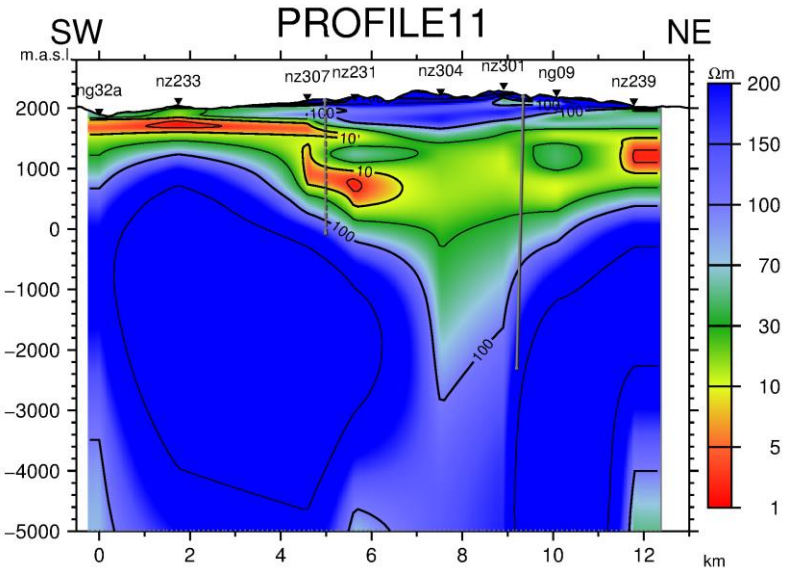

Figure 11: Resistivity cross-section along profile 11 (location on Figure 7). Grey straight line is the projection of the inferred fault mapped on surface and the doted line represents the south extension of the same fault.

5.1.5 Resistivity cross-section along Profile 12

Profile 12 is located 5,600 m northwest of Ngozi Caldera Lake (see Figure 7). It was made to trace further the extension of the fault mapped on profile 11 located about 1,800 m south where the fault is observed to have little displacement in the resistivity anomalies. The main visible features are:

i. A thin surficial resistive > 100 Ωm layer thinning away from the centre.

ii. A 100 Ωm anomaly about 100 m thick between MT station nz230 and nz225 below the resistive surficial layer

iii. The very extensive high conductive < 10 Ωm layer below the surficial resistive layer with thickness ranging between 400 m and 1,000 m. This layer is deep and thick in the central part of the cross-section and is more elevated towards SW where it is covered by thin resistive layer.

iv. A resistive > 100 Ωm thick zone with top part defined by a 100 Ωm iso-resistivity line extending to great depth.

v. A 30 -70 Ωm resistivity anomaly at greater depth of about 4,000 m b.s.l. revealed below MT station nz224

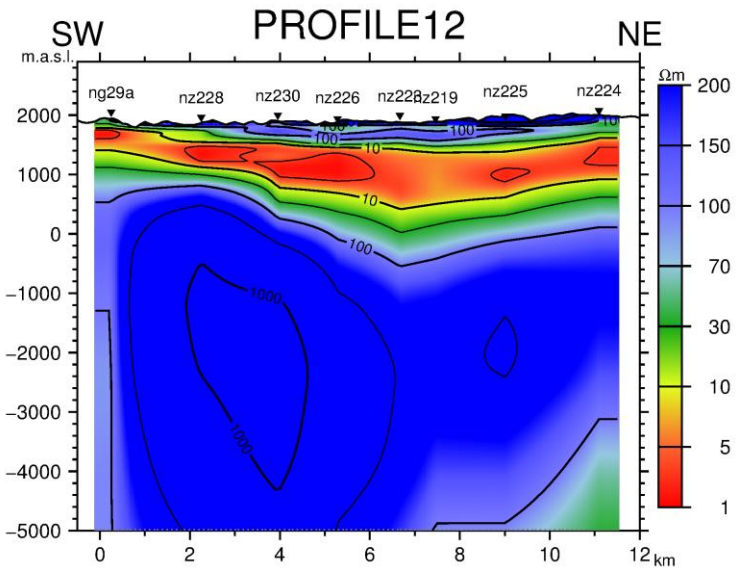

Figure 12: Resistivity cross-section along profile 12 (location on Figure 7).

5.2 Resistivity Depth Slices

Resistivity depth slices presented in this study were generated by the TEMRES program (Eysteinsson, 1998). They were generated from the jointly inverted MT-TEM sounding data, the 1D Occam models with the objective to understand the general lateral trend of the resistivity distribution at different depths throughout the entire surveyed area of the Ngozi prospect. As indicated on the location map (Figure 7), there is a gap without MT-TEM stations close to Ngozi caldera because of accessibility difficulties. This gap reflects uncertainty in the understanding the general trend of resistivity below the caldera where the high temperature manifestations are found. Therefore, interpolating resistivity models around the caldera means uncertainties. Here, a few selected resistivity depth slices are discussed, at 1,500 m a.s.l, 1,000 m a.s.l and 500 m a.s.l for interpretation purposes. More maps can be found in Appendix 3 in Didas, (2018).

5.2.1 Resistivity map at 1,500 m a.s.l

The map was generated with the objective of determining the lateral extension of the conductive anomaly < 10 Ωm in the area which is thought to be the alluvial clay rich sediments deposited within the paleo-basin trending NW-SE in the area. The main visible features are:

i. A conductive anomaly < 10 Ωm trending NW-SE west of Ngozi caldera. From south to north the anomaly is truncated by a > 10 Ωm anomaly.

ii. A resistive > 100 Ωm anomalies incising east and southwest of the map which could be representing the low permeable formations less or not affected by geothermal alterations in the area.

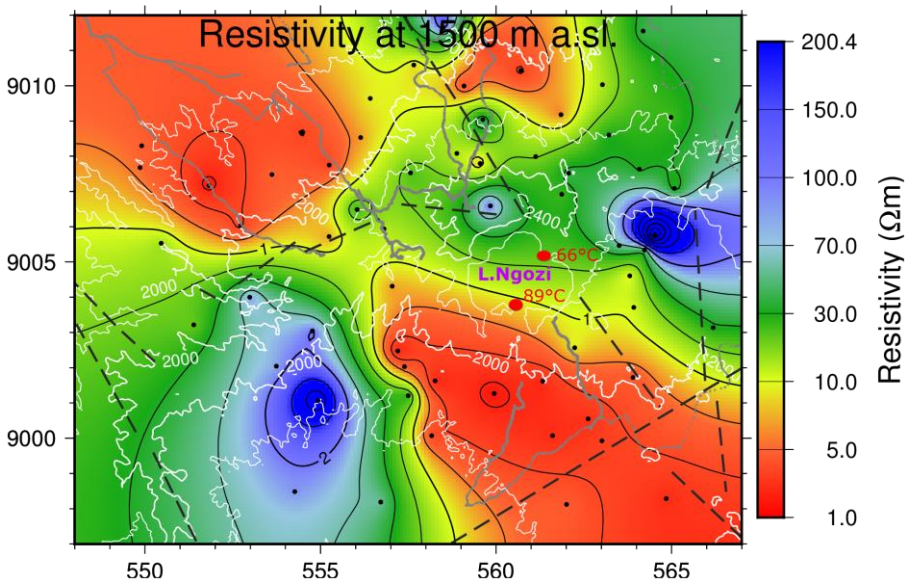

Figure 13: Map showing the lateral resistivity distribution at a depth of 1,500 m a.s.l. The grey lines are the accessible roads and field tracks and black dotted lines are the inferred faults mapped on surface. Black dotes are MT stations and the red dotes are the hot springs located at the bottom of Ngozi Caldera Lake indicated by the circular contour line. The resistivity contours on the map are in logarithimic scale.

5.2.2 Resistivity map at 1,000 m a.s.l

This map was generated primarily to investigate the lateral extent of the base of the conductive <10 Ωm anomaly and secondly to investigate the lateral extent of the top of moderately resistive anomaly thought to be the top of the geothermal reservoir in the area. The following are the main visible features in the map:

i. Distinct very conductive <10 Ωm anomalies located south and north of the moderately resistive anomaly 10-50 Ωm probably representing the bottom patches of the clay rich formations.

ii. A well-defined NW-SE trending anomaly characterised by moderately intermediate resistivity 10-50 Ωm values engulfing the Ngozi caldera lake, probably representing the top part of the reservoir.

iii. Two high resistive >100 Ωm core anomalies bounding the moderately resistive anomaly to the east and west respectively, representing the low permeable zones likely to be the metamorphic basement.

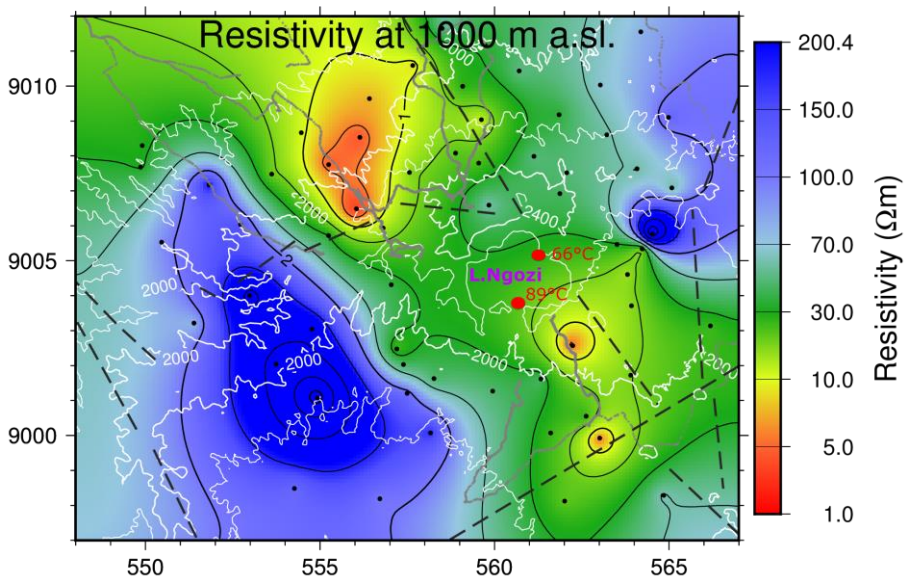

Figure 14: Map showing the lateral resistivity distribution at a depth of 1,000 m a.s.l. The grey lines are the accessible roads and field tracks. The black doted lines are the infered faults mapped on surface. Note; the resistivity contours in the map are in logarithimic scale.

5.2.3 Resistivity map at 500 m a.s.l

A resistivity map at 500 m a.s.l was generated to investigate the lateral extent of the moderately resistive anomaly 30-70 Ωm observed in most of the cross sections, bounded to the east by the inferred fault mapped on surface. The secondary objective was to investigate the western end of this fault which is now clear in the map (Figure 15). The visible features are:

i. An intermediate conductive anomaly 30-70 Ωm, clearly visible in the central part of the survey area which is in good agreement with the NW-SE trending inferred fault zone mapped on surface. Similarly, it engulfs the Ngozi caldera lake and extends further to the north and south. Considering the presence of the hot springs in the Ngozi caldera, the fault zone is likely to be controlling the high temperature geothermal system in the area as manifested by its low resistivity values relative to the surrounding area. The low resistivity within the fault zone is an indication of hermetically closed high permeability zone which could be an important production zone.

ii. The eastern and western part of this anomaly (? fault zone) is dominated by a high resistive core with resistivity value of > 100 Ωm which is in agreement with the low permeable metamorphic basement.

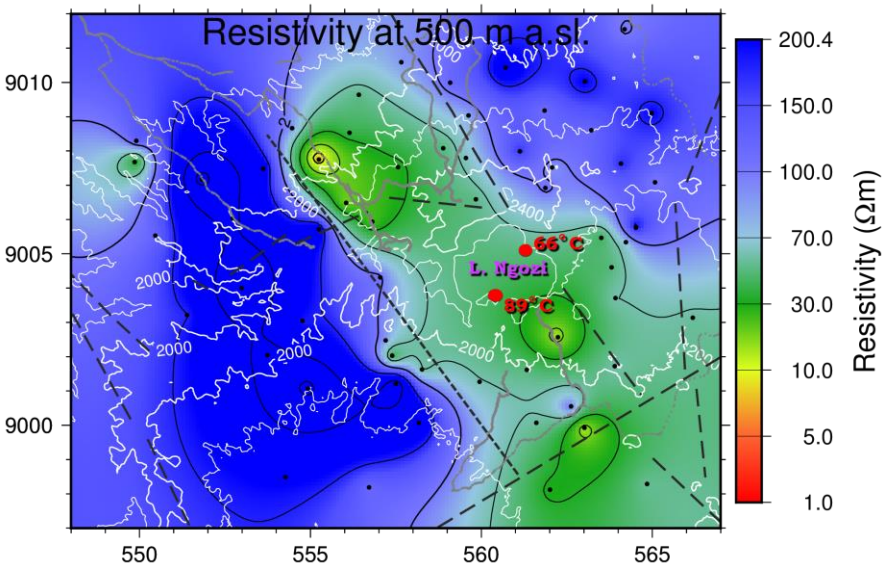

Figure 15: Map showing the lateral resistivity distribution at a depth of 500 m a.s.l. The slice cuts through the middle portion of a probable reservoir hermatically closed within the fault. zone. The resistivity contours on the map are in logarithimic scale. Figure caption is shown on Figure 13.

9.3 Strike and induction arrows analysis for 2D/3D Dimensionalities of the data

The geo-electrical strike direction gives information about the 2D resistivity structure; in which direction the resistivity changes the least. In 2D Earth model the resistivity varies with depth and in one horizontal direction. The strike direction is represented by the induction arrows or strike rose diagrams generated from the vertical magnetic field Hz, Tipper tensors for each MT station. Since the Tipper is a complex vector, it may simply be represented as induction arrows of the real part and the imaginary part. As described by Parkinson, 1959; Berdichevsky and Dmitriev, 2002, the real induction arrows are used and is presented below. According to Parkinson convention (Parkinson, 1959; Berdichevsky and Dmitriev, 2002), the imaginary part is sensitive to resistivity contrasts close to the measurement site while the real part is more sensitive to regional resistivity contrast. The real induction arrows point towards regions characterized by current concentration i.e. high conductivity and towards a zone of low conductivity. The imaginary part is normally pointing away from a zone of high conductive body towards a zone of resistive zone. This is because the imaginary part is always more sensitive to resistivity close to the measurement site and the real part to broader resistivity contrast. The size of the arrows depends on the magnitude of the vertical magnetic field. If the magnitude of the vertical magnetic field is small the induction arrows will be small and vice versa.

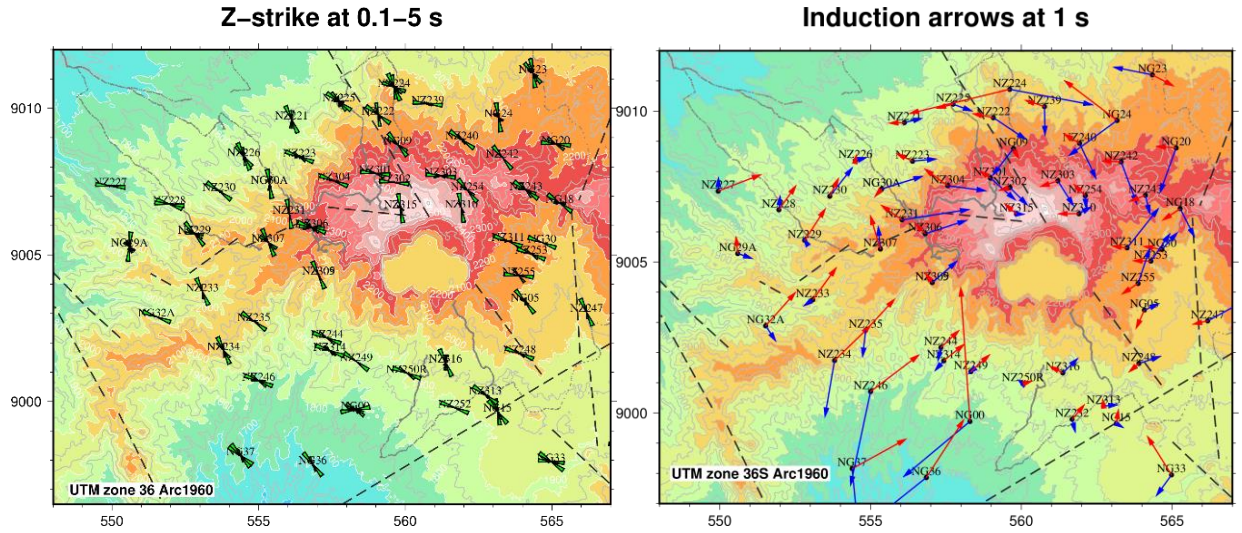

Figure 16: Induction arrows for the period of 1 s. The blue arrows are the real part and the red arrows are the imarginaly part. Zstrike for the period of 0.1 to 5 s.

For 2D Earth the real and imaginary arrows are co-linear and point perpendicular to the strike of the 2D geoelectrical structure (Berdichevsky and Dmitriev, 2002). However, asymmetry of the medium violates the collinearlity of the real and imaginary parts and thus, the real and imaginary part point in different directions. The horizontal direction perpendicular to directions of the imaginary and real part is called the geoelectric strike (Hersir et al., 2015). The angle which the geoelectric strike makes with the geographical north is called Swift-angle or Zstrike. The Zstrike direction is found by minimizing the diagonal elements of the impedance tensor, in such a way that Zxx=Zyy=0 or maximizing the off diagonal elements, in such a way that Zxy ≠ -Zyx. The shortcoming with this method is that there is 90º ambiguity in in geoelectric strike. This problem is resolved by measuring the vertical magnetic field, Hz which is generated by lateral conductivity gradients and calculating the Tipper (Hz=TxHx+TyHy) (see Schmucker, 1970) which relates the vertical components of the magnetic field to its horizontal components and the strike is obtained by minimizing |Tx| (Vozoff, 1991). The Tx and Ty are the x and y-components of the Tipper, respectively. In 1D resistivity structures there is devoid of excess currents. Hence, the vertical magnetic field component and the Tipper are zero, where as an Hz can be induced in 2D and 3D cases due to excess currents caused by horizontal variations in the electric currents (Berdichevsky and Dmitriev, 2002).

The importance of the electrical strike direction is that it gives valuable information on the subsurface fractures and permeability not necessarily seen on the surface which are an important additional information for confirmation of the model and in developing the conceptual model and siting of wells. The strike is a function of frequency and thus, different for different depths.

In this study the geo-electric strike analysis of MT data was performed to investigate potential permeable zones which could help in revising the existing conceptual model. To make this viable, multi-frequency plots of the strike and induction arrows inferring different depths for each MT sounding are plotted on a map shown on Figure 25 and 26. For clarity two maps are presented in this section but more maps can be viewed in Didas, (2018).

From the strike analysis shown in Figure 25 above it can be observed that for period of 1 s, the real induction arrows point towards the more conductive zone close to Ngozi caldera. Using the Zstrike (Figure 26) the main electric strike is found to be NW for most of the Ngozi MT stations. This trend is parallel to the fault zone mapped in this study (Figure 24) also observed from the geological map of the area (Figure 16).

5.4 Geothermal interpretation of the results

A geothermal system consists of convection of water in the upper crust of the Earth in a confined space and there it transfers heat from the heat source (e.g. shallow magma chamber or hot intrusive bodies) to the heat sink usually the free surface. Thus, a

geothermal system is made up of three main elements: heat source, a reservoir and fluid, which is the carrier that transfers the heat. The geothermal reservoir is normally separated from the uppermost rocks by an impermeable relatively thick rock layer composed of smectite clay minerals as a result of geothermal fluid-rock interaction. In resistivity survey particularly MT, the elements of the geothermal system can be observed. The clay cap is normally very conductive, the reservoir is moderate resistive and the heat source (if any present) below the reservoir is conductive. The rocks (cold rocks) not affected by geothermal processes normally give the highest resistivity signatures.

The high temperature geothermal field in Ngozi area is characterized by the following resistivity structures. From surface, it is characterized by the high resistive > 100 Ωm unit overlying a conductive cap which overlies a resistive core. Linking this unit to the geology of the area, the high resistive unit from the surface is the ash-pumice (with thickness reaching over 1 km) with low or no alteration. The prominent highly resistive bodies with its top part defined by a 100 Ωm iso-resistivity line and extends at greater depths is interpreted as low permeable Precambrian metamorphic basement.

The < 10 Ωm conductive layer in cross-section 5 (Figure 8) is the clay cap. The moderately resistive zone of 30-70 Ωm below the conductive layer with thickness of about 1,500 m centred at 500 m a.s.l could be the geothermal reservoir with high temperature clay minerals like epidote, chlorite and amphibole formed at a temperature greater than 230°C. A localized possible heat source is observed as the very conductive < 10 Ωm patches within a vertical conductive anomaly of 10-30 Ωm, (5 km wide) imaged below MT stations ng00 and nz316 in cross-section 5 (Figure 8). This is probably some hot intrusives within the fault zone being fed by the magma chamber located several kilometres below the reservoir. Similar signature is anticipated below the Ngozi caldera where the indicative high temperature hot springs discharge at the bottom of the lake. However, there is no MT sounding to constrain this observation.

The upper part of the intermediate resistive anomaly of 30-70 Ωm below the surficial resistive layer within the fault zone is likely to be a poorly developed clay cap of the geothermal system possibly composed of smectite-Illite formed at a temperature between 50 and 200°C. It is difficult to clearly set a boundary between the clay cap and the reservoir except for profile 5 (Figure 8). The shallow-subsurface conductive horizontal anomaly located east, west and far north of the fault zone and the Ngozi caldera is interpreted as clay rich sediments which was deposited within the NW-SE trending paleo-basin (see Figure 13) with considerable amount of conductive minerals of sedimentary origin or partly formed by alteration, like kaolinite, smectite and zeolite that have high Cation Exchange Capacity (CEC). It is likely that, the sediments might have also been affected by geothermal alteration but this would be an outflow before the development of the Ngozi caldera. It is also likely that, after the development of the caldera the geothermal system is hermetically isolated within the fault zone identified in this study. The eastern flank of the identified fault zone was mapped during geological mapping campaign by Alexander et al. (2016) but the western arm has never been mapped except in this study.

6. INTEGRATED INTERPRETATION OF THE RESULTS

Integrated interpretation here means eventually, attaching the geological and geochemical labels (realities) from the previous studies to the MT results in this study to get the meaning of geothermal system of the area. The aim is to constrain their relationships, update the conceptual model and define the high priority area and propose some exploration drilling targets.

6.1 The cap rock, reservoir and heat source

The resistive surficial layer (see the MT cross-sections) can be correlated with the ash-pumice which is covering large parts of the prospect (see Figure 3 and 7). The underlying conductive layer within the fault zone correlates to the poorly developed smectite-illite clay cap formed at a temperature between 100°C and 230°C in the geothermal system. The smectite-illite clay cap does not extend further east of MT station nz248 located close to escarpment of the inferred thrust fault dipping towards southwest (see Figure 8). Similarly, the vertical conductive anomaly zone revealed by MT stations nz250, nz316, MBY407 and nz248 almost terminates at station nz248 where the mapped fault escarpment is located.

The base of the clay cap direct above the fault zone (and possibly hosting the heat source) is relatively elevated (up-doming) due to tendency of the smectite to transform to more resistive illite and chlorite, clays characteristics of permeable reservoirs (see Figure 8). Similar phenomenon is described by Anderson et al. (2000) and Cumming (2010).

The imaged fault zone if active is likely to allow heat flow from the shallow heat source to the high temperature reservoir (> 230°C) above and the occurrence of the concealed hot springs at the bottom of the Ngozi Crater Lake indicating the subsurface geothermal activity within the fault zone (see Figure 15). Fracture permeability mainly within the fault zone controls the fluid flow. The locally elevated clay-cap just west of the conductive fault zone and east of the Shiwaga gas vent observed in cross-section 5 (see Figure 8) could be attributed by cooler inflow of cold fluids from west thus, resulting in local increase in resistivity at the base of the clay cap. Similar phenomenon is described by Cumming (2009b, 2010). As, it has been reported by de Moor et al. (2012), the CO_2 and He gases from Shiwaga gas vent are of Mantle origin. Therefore, we preclude the link to the geothermal system observed east of the gas vent along profile 5 of this study.

It is likely that the conductive fault zone imaged at MT station nz316 in cross section 10 (see Figure 10) is the same fault which extends further towards the Ngozi hot springs also manifested by the lineament mapped from the remote sensing data (see Figure 7). The same fault is evident north of the Ngozi Caldera Lake along cross sections 9 and 11(see Figure 9 and 20).

The presence of the two extensive border faults to the east and west of the Ngozi Caldera (2.5 km long and 1.6 km wide, and 74 m depth) would prevent significant leakage of the fluid from the high temperature reservoir away from the fault zone except within the fault zone itself where the clay cap is fractured by faulting for example at the bottom of the Ngozi Caldera Lake. This implies a hydrologic sealing off of the high temperature geothermal system from its surrounding (see Figure 15).

The Shiwaga gas vent located at the phonolite and sandstone interfaces indicates a deep-seated fault separating the two formations and possibly a special constrained conduit which brought magma that cooled to form phonolite. It is likely that the fault is associated by the very extensive NW-SE trending Mbeya Front Range fault (a fault connecting Matula spring) located 3 km west of imaged geothermal system and is likely to be the important concealed fault towards the Shiwaga gas vent but very evident northwest of this location (see Figure 7). This fault if extrapolated further south will pass through the Shiwaga gas vent.

The contact between the old volcanic rocks and the metamorphic basement is marked by the 100 Ωm iso-resistivity line. In general, the Precambrian metamorphics are the most resistive rocks in the area and this indicates that they are impermeable rocks not affected much by geothermal alteration except within the fault zone (see Figure 15).

The absence of the up-doming of the clay cap close to the Ngozi Caldera could be attributed to its destruction caused by collapse during the caldera formation.

The adjacent conductive zones of clay rich sediments truncated by faulting to some extent could also be affected by an outflow extending laterally for some distance before the formation of the caldera contemporaneous with the hydrologic sealing off the geothermal system within the zone of opposite dipping fault boundaries trending NW-SE.

The absence of a very conductive cap within the fault zone close to Ngozi Caldera could be attributed to two possible causes:

i. Absence of the clay rich sediments removed during volcanic eruption phases from the Ngozi volcanic center contemporaneously with the development of the geothermal system. The portion of the sediments removed were occupied by trachyte volcanic rocks which has low magnesium content. These rocks were subjected to geothermal heating and undergone alteration to form a mixed layer-clay cap composed of smectite-illite-chlorite which normally is not very conductive. The formed clay cap gradually was destructed by faulting during the formation of the Ngozi Crater or Caldera.
ii. Another possible explanation is that the smectite clay during the collapse of the mouth of the volcano to form the caldera were buried and heated at greater depth and there was converted into mixed clay layer composed of mixtures of smectite-illite hence increase in resistivity. Thus, based on this assumption, it is likely that there is no elevated clay cap even very close to the Ngozi Caldera.

The vertical conductive anomaly imaged in cross-sections 5 and 10 (see Figure 8 and 10) is an important signature indicating possible heat source located at a depth between 4 and 5 km within the fault zone. The very conductive patches in the vertical conductive zone could be the young hot intrusives associated to the caldera structure (<1 ka) conductive supplying heat within the fault zone. However, a 3D inversion model is needed as a quality assurance step to test this imaging uncertainty at greater depths. This is because most of the data in the area have 3D effect at greater depths. However, in correlating the averages from the resistivity as proposed by Park and Livelybrook, (1989), all the four MT stations imaged the vertical anomaly show the same value hence the Earth is assumed to be 1D around this anomaly (for more information for the reader see Appendix 2 in Didas, 2018).

The conductive anomalies located east of the inferred fault could be fossil geothermal system (or series of small systems) and possibly the peripheral outflow of the Ngozi geothermal system before was hermetically isolated enclosed within the fault zone as it is observed in this study with the most promising geochemical evidence of > 230°C upflow at the bottom of Ngozi Caldera Lake.

The thick volcanic ash-pumice reaching a thickness of more than 500 m within the fault zone might have the root course for masking the surface geothermal manifestations except below the Ngozi caldera lake where there likely to be intense fracturing of the clay cap by faulting.

The preferred interpretation of this study is that the base of the argillically-altered volcanic formation uncomformably overlies the Proterozoic metamorphic basement complex except within the fault zone which corresponds to the upflow zone (observed below Ngozi caldera lake) of the hermetically closed geothermal system in the area. Similarly, the alluvial sediments overly either older volcanics or the metamorphic basement in low elevated areas.

There is a big uncertainty with most of the surface mapped faults whether they are normal or strike slip faults since no movement have been described on these faults. This is because the area is covered by thick deposits of pyroclastic material forming unconsolidated ash-pumice. So, most of the faults in the area are inferred and some of them were interpreted as lineaments. However, the resistivity results from this study have been an important tool for the good correlations with the inferred geological structures. It is good to point out that, whenever, there is a displacement of the shallow conductive anomalies in MT cross-sections, at the surface, the geologist were at least able to map either an inferred fault, a shear zone or a lineament. Examples of these correlations is observed at profile 2, 3, 4, 5, 8, 9, 10, 11, 13, 14, 15, 16 and 17 (see Appendix 3 in Didas, 2018).

6.2 Areal extent of the reservoir

The northeast limit of the reservoir clearly coincides with the very extensive (over 20 km long) NW-SE trending inferred fault mapped on surface during geological survey by Alexander et al. (2016) in the study area. This fault zone from northwest to southeast connects the Ngozi Rungwe and Kiejo main volcanic centers and was disturbed by the NE-SW fault with right lateral strike slip movement (see Figure 7 and 17) south of profile 3 (Alexander et al., 2016). The northwest extension limit of this fault was not mapped on surface during geological mapping campaign but is clearly observed in MT resistivity anomaly in cross-sections 5 and 9 (Figure 8 and 9) located about 2 km south and north, respectively, of the Ngozi caldera lake. The width of this fault ranges between 4 km at shallow depth and 7 km in greater depths. The northeast extension limit of the extensive fault zone mapped on surface is indicated by the dislocation of the smectite clay-cap with significant downward movement at MT station nz305 while its northeast extension limit is terminated at the inferred fault at MT station nz302. The lateral distance between MT station nz305 and

nz302 is about 4 km, similar to that mapped in the south of the Ngozi caldera in cross-section 5 between MT station ng00 and nz248.

This fault zone has small deformations beyond cross-section 9 (Figure 10) as observed in cross-section 11 (Figure 11) and does not extend through profile 12 (Figure 12). This is clearly observed in cross-sections 11 (Figure 11) and 12 (Figure 12) where the shallow conductive layer might be associated with the clay rich sediments deposited in the rift basin with no or little effect of geothermal interactions. In considering the above observations, the northeast and northwest extension limits of the reservoir is assumed to be within the fault zone of 4 km maximum width over a total of 7 km long with limited extension about 2 km north from Ngozi Caldera Lake.

The estimated areal extent is obviously related to the fault fracture permeability assuming that the fluids ascending along this fault zone spread over laterally more to the northwest and do not escape from the fault zone either to the east or west. Thus, the geothermal system is hydrological closed off within the mapped NW-SE trending inferred fault acting as the major barrier to the east and its western concealed boundary being the barrier to the western leakages of the geothermal fluids which is NaCl in composition. This observation is supported by the absence of the mixing of chlorine water escaping from the reservoir hosted in the fault zone and manifested by the hot springs below the Ngozi Caldera Lake. Thus, as pointed out in the geochemical report chapter of Alexander et al. (2016), that the hot springs located west of the identified fault zone is from the conductively heated basement rocks and has no mixing with the NaCl water from the high temperature geothermal reservoir located below the Ngozi Caldera. By adopting the above mentioned parameters, the first priority zone, represented in Figure 26, has an area extent of 28 km^2.

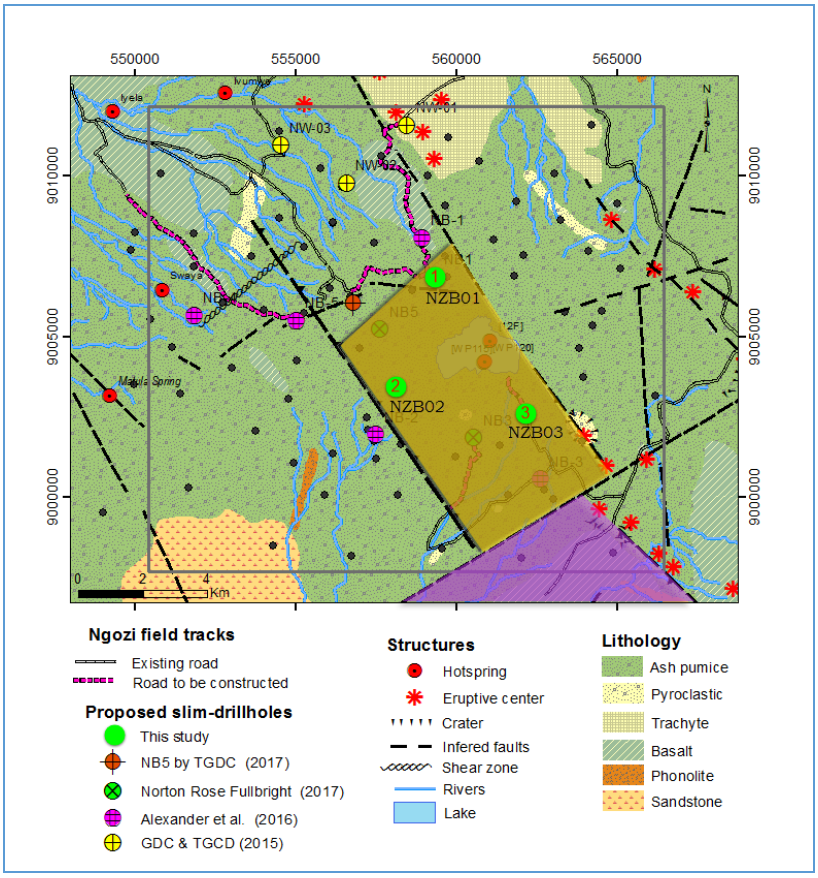

Figure 17: Areal extent of the geothermal reservoir. The first priority zone is the orange zone (zone in the midle bounded by faults and Magenta coloured zone (lower right corner) is the second priority zone. The numbered Green circles are the proposed drilling sites from this study. The black dotes are the MT-TEM stations

6.3 Top of the reservoir

The depth to the top of the reservoir is interpreted based on the results of the 1D resistivity model shown in profiles 5, 9 and 10 assuming iso-resistivity line of 70 Ωm as the contact between the cap rock and reservoir, the top of the reservoir is regarded at a depth of 1,000 m b.g.l but becoming deep towards the Ngozi caldera reaching a depth of 1,500 m b.g.l north of the caldera. This is likely to be associated with the collapse during the caldera formation as obviously indicated in the cross-section along profile 9.

6.4 Bottom of the reservoir

The bottom of the reservoir is not resolved in most of the cross-sections in the area except for the cross-section along profile 5 where the bottom of the reservoir is assumed to correlate with the iso-resistivity line of 30 Ωm above the vertical conductive anomaly within the fault zone interpreted in this study as the heat source. Thus, the bottom of the reservoir is assumed to be at a depth of -600 m b.s.l and the thickness of the reservoir is approximated to be in the order of 1,500 m.

6.5 Vertical extent of the reservoir

Based on the information obtained in the MT survey of the top and the bottom of the reservoir as just described above, the thickness of the reservoir is approximated to be in the order of 1,000 m and 1,500 m.

7. A REVISED NGOZI GEOTHERMAL CONCEPTUAL MODEL

An integrated conceptual model of Ngozi geothermal system (Figure 18) is developed in this study with the view to target sites for possible exploration wells. The geothermal system is hermetically closed within the convective fault zone.

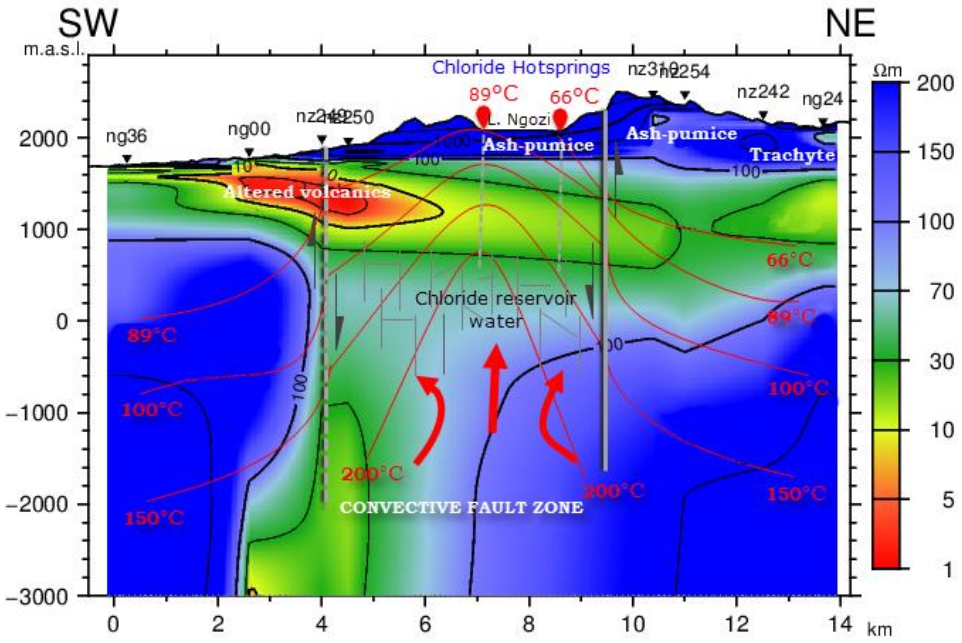

Figure 18: A reviced geothermal conceptual model of Ngozi prospect. The grey line is the mapped fault and the dotted line represents the extension of the same fault observed in this study.The curved lines are isothermal linesand the thick allows indicates the heat flow within the fault zone.

8. PROPOSED DRILLING TARGETS

The location of the proposed test drilling targets (shown in Figure 17 and 19) are based on the integrated interpretations results of the geological, geochemical resistivity model. All three datasets are observed to have a very good correlation in this study as already described in the previous chapter. All the first three test drilling targets **NZB01**, **NZB02** and **NZB03** are located within the fault zone observed from this study. Drilling site **NZB01** is located about 1,800 m north of the Ngozi caldera to test the northern extension of the resource hosted in the fault zone (see Figure 16). **NZB02** is located about 2 km south of the Ngozi caldera lake to investigate the southern extension of the resource while **NZB03** is located west of the Ngozi caldera to test the western extension of the same geothermal reservoir observed in MT soundings of this study. All the three proposed drilling sites can be accessible by conversional drilling rigs as reported by TGDC (2017) ground truthing internal report and the field survey roads shown on the map in Figure 16. **NZB01** is located at the same location as **NB-1** previously proposed by Norton Rose Fulbright (2017). **NZB03** is located about 2,000 m north of **NB-3** proposed by Alexander et al. (2016) and drilling site **NZB02** from this study is located about 2 km northeast of the **NB-02** proposed by Alexander et al. (2016), 3 km southwest of **NB-5** proposed by Norton Rose Fulbright (2017) and about 2.5 km southeast of the re-located **NB-5** by TGDC (TGDC, 2017). The proposed drilling site **NZB02** will need further ground truthing verification since there was no ground truthing survey by TGDC (2017) to this location.

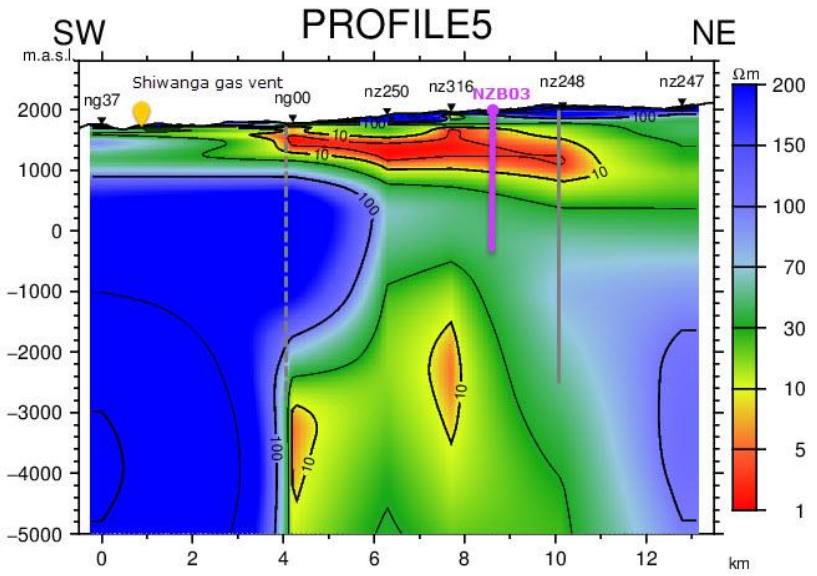

Figure 19: Proposed drilling target NZB03 (thick line) from this study. The grey full and dashed lines are the mapped faults

9. ESTIMATED RESOURCE CAPACITY – VOLUMETRIC ASSESSMENT

An assessment of the geothermal resource in Ngozi prospect has been estimated using lognormal power density approach which provided most of the input parameters needed for Monte Carlo stored heat assessment within a defined reservoir volume (i.e. heat stored in the rock matrix and heat stored in the reservoir fluid). This approach then estimates how much of that heat can reasonably be extracted and converted to useful power using typical technology (i.e. recovery factor). The lognormal power density approach for undrilled prospect like Ngozi first requires an estimate of temperature of the reservoir based on geochemistry, porosity of the reservoir, area extent of the reservoir, thickness of the reservoir, recovery factor, Load factor, density of water, specific heat capacity of the reservoir rock and cut off temperature (Wilmarth and Stimac, 2015; Cumming, 2016a).

A resource area in this study is estimated based on MT resistivity data, geological and geochemical results and interpretations. The reservoir was observed to be hosted in a fault zone, 7 km long and 4 km wide and thus making an area of about 28 km2. Estimates of selected input parameters are described below and summarized in Table 1.

i. Resource areal extent of 28 km2 hermetically isolated within the fault zone (see Figure 17).

ii. Thickness of the reservoir ranging between 500 to 1,500 m based on the geological and geophysical conceptual models. Assuming that the base of the clay cap is at 1,000 m a.s.l as observed in MT cross-sections 5 and 9 located south and north of the Ngozi caldera, respectively.

iii. An average equilibrium temperature of the reservoir 232±13°C based on geothermometry estimates. So, the maximum value, including the error range is 232+13 or 245°C and the Minimum value is 232-13 or 219°C

iv. Effective Porosity between 3 and 8% inferred as a typical volcanic effective porosity for fractured volcanic rocks (older volcanic rocks on top of the basement in Ngozi prospect).

v. Cut off temperature of 89°C which is the temperature equivalent of the hot spring discharging below the Ngozi caldera lake.

vi. Recovery factor of between 5% (minimum) and 20% (maximum) with the best value being 12% of the stored heat within the reservoir.

Table 1: Estimates of selected input parameters for volumetric assessment of the heat stored in the reservoir rock.

INPUT VARIABLES	UNITS	MIN	BEST VALUE	MAX	PROBABILITY DISTRIBUTION
Area	km^2	2.9	N/A	28	Constant distribution
Thickness	m	500	1000	1500	Constant distribution
Rock density	kg/m^3	2700	2700	2700	Fixed value
Porosity	%	3	5	8	Triangular distribution

INPUT VARIABLES	UNITS	MIN	BEST VALUE	MAX	PROBABILITY DISTRIBUTION
Area	km^2	2.9	N/A	28	Constant distribution
Recovery factor	%	5	12	20	Triangular distribution
Rock specific heat	J/kg °C	N/A	900	N/A	Fixed value
Temperature	°C	219	232	245	Triangular distribution
Fluid density	kg/m3	N/A	864	N/A	Fixed value
Conversion Efficiency	%	11.5	15.4	16.3	Triangular distribution
Fluid specific heat	J/kg °C	N/A	4510	N/A	Fixed value
Plant life	years	N/A	30	N/A	Fixed value
Load factor	%	N/A	95	N/A	Fixed value
Rejection Temperature	°C	N/A	80	N/A	Fixed value

High (P90), Median (P50) and Low (P10) values for temperature and resource area are estimated. Finally, the power capacity distribution of the resource is computed from the product of the resource area and power density distributions all of which are assumed to be lognormal as indicated by the geothermal field population. The results of the volumetric assessment indicate that the electric generation capacity of Ngozi corresponds to 49.4 MWe power generation for 30 years with a 90% confidence level.

The mean capacity for the same period is estimated 137.1MWe (Figure 20 and 21). The 90% confidence range observed in the simulation result takes into account the uncertainties arising from insufficient knowledge about the reservoir conditions. As stated by Grant (2015) and Garg and Combs (2011) if the parameters above are overestimated; particularly the average resource thickness and recovery factor commonly results to the inflated Monte Carlo stored heat calculations.

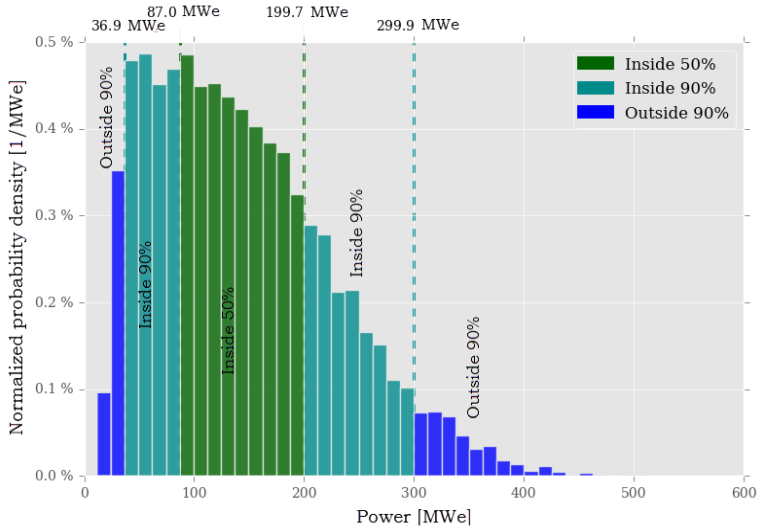

Figure 20: Probability distribution for electrical generation capacity for Ngozi geothermal field assuming 30 years of operation.

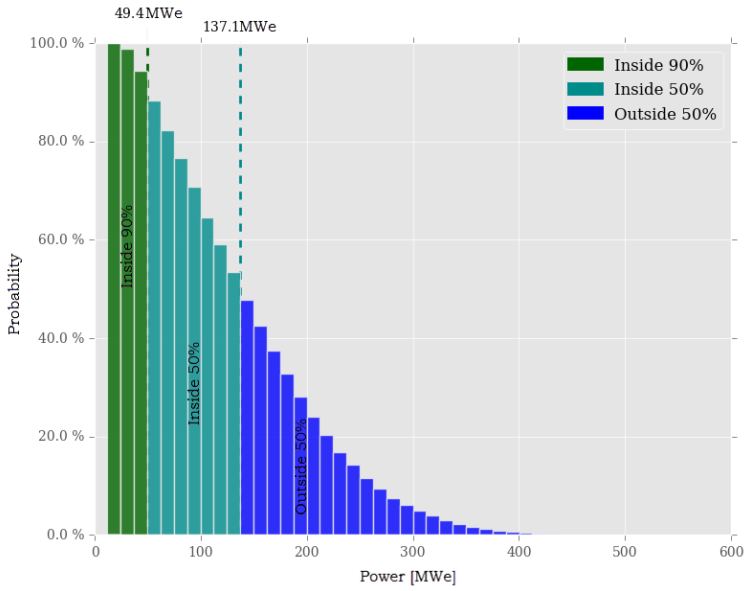

Figure 21: Cummulative probability distribution for electric generation capacity for Ngozi geothermal field assuming 30 years of operation.

10. CONCLUSIONS

The present study can image the existence of a geothermal resource in the Ngozi prospect and define its extent. The resource is extensive and is hosted within a 4 km wide NW trending fault zone which is about 7 km long from the south and crosses Ngozi Caldera. The fault zone engulfs the Ngozi Caldera Lake together with the hot springs located at the bottom of the lake. A possible heat source is shallow intrusives, which are observed within the fault zone at a depth of 3.5 to 4 km bsl and seems to extend towards the Ngozi Caldera. Beyond 2,000 m northwest of the Ngozi caldera, there is limited indication for the extension of geothermal resource. The only indication is the thick extensive very conductive layer which extends throughout the profiles e.g. along profile 12. Such thick 500 -1,000 m continuous layer could be mainly associated with the clay rich sediments filling the depocenters with possible little interaction with geothermal activity. This observation gives the impression that the geothermal resource does not extend more than 2,000 m northwest of the Ngozi caldera. Unlike the previous studies, the current results are supported by both the geology and geochemical results. The fault imaged from MT data is also mapped on surface during geological survey. This fault acts as the boundary for the geothermal resource to extend further west and the clay cap from south to north of the Ngozi caldera terminates along this fault. Similarly, the fault seems to connect the hot springs present below the Ngozi caldera which is the only geochemical indicator for the existence of the high temperature geothermal system with the reservoir temperature of 232°C from Na-K geothermometers.

Other important link observational is the Shiwaga CO_2 gas vent emitting significant amount of predominant magmatic CO2 gas and the resistivity anomalies. From resistivity observation this vent is located in the peripheral part of the high temperature geothermal system and it is likely that the peripheral part of the system is cooling down as it interacts with deep cold formations in the west. However, it is also likely that the deep fault which brings such significant amount of CO_2 to the surface could not be linked to the high temperature geothermal system imaged in this study. This is because there have been several studies which concluded the origin of the CO_2 gases in the regional to be originating from deeper mantle sources including the one mined at Kiejo.

Whether the alteration is in equilibrium with the temperature at present, will only be verified by drilling. However, the geothermometry study from Na-K of the hot springs sampled at the bottom of the Ngozi Caldera Lake gave reservoir temperature value of 232°C. This temperature is enough for power generation in steam turbines.

The lack of MT/TEM stations close to Ngozi Caldera masks important information below the Caldera. This would have helped much to constrain the geothermal system below the Caldera where the only indication of high temperature geothermal system was found.

11. RECOMMENDATIONS

- Select survey area, which consistently shows a geothermal system and do systematic MT/TEM infill.
- Perform 3D inversion of static shift corrected MT data in the selected areas as quality assurance step to test the 1D imaging and to better define the resistivity anomalies especially the deep conductive anomaly imaged in 1D model which is interpreted in this study as a heat source hosted within the large and extensive NW trending fault zone.
- Perform 2D inversion with the purpose of imaging/modelling the conductive anomaly below the shallow conductive anomaly within the fault zone identified in this study.
- Focus systematic, structural, and geological mapping of the area so as to reduce the uncertainties of the mapped faults. This is because most of the mapped faults are inferred or lineaments from remote sensing data.

- Conduct MT/TEM survey infilling gap filling close to nz316, nz315 and near the Ngozi Caldera in order to confirm the extension of the updoming clay cap mapped at nz316 and fault zone which was observed to continue towards the Ngozi hot springs located at the bottom of the lake.

AKNOWLEDGEMENTS

The Authors wish to thank Tanzania Geothermal Development Company Limited for supporting this work through providing the data and reference materials. We are indebted to United Nations University-Geothermal Training Program in Iceland for the financial and technical support that enabled this work. The authors benefited from thoughtful discussion with William (Bill) Cumming, Knútur Árnason and Ásdís Benediktsdóttir

REFERENCES

Alexander, B.K., Cumming, W., and Marini, L.: Geothermal resource assessment report. Ngozi and Songwe geothermal prospects, Tanzania. Final report-September 2016. TGDC technical internal report. Unpublished, (2016) 695 pp.

Árnason, K.: TEMTD, A Programme for 1D inversion of central-loop TEM and MT data. Short manual. ÍSOR, Iceland Geosurvey. Unpublished, (2006) 17 pp.

Árnason, K.: TemX, short manual. ÍSOR, Reykjavík, internal report, (2006a), 17 pp.

Árnason K.: Central loop transient electromagnetic sounding over a horizontally layered Earth. Orkustofnun, Reykjavík, Report OS-89032/JHD-06, (1989) 129 pp.

Bendat, J.S., and Piersol, A.G.: Random data: analysis and measurement procedures. New York, John Wiley (1971).

Chave, D.A., Robe L.E., Ian, J.F, Alan, G.J., Randall, L.M., William, L.R., Ari, V., and Peter, W.: Introduction to the magnetotelluric method. Cambridge University Press (2012), 1-14

Cumming, W., and Mackie , R.: Resistivity Imaging of geothermal Resources using 1D, 2D and 3D MT inversion and TDEM static shift correction illustrated by a Glass Mountain Case History. Proceedings World Geothermal Congress, Bali, Indonesia (2010).

Cumming, W.: Resource capacity estimates using log normal power density from producing fields and area from resource conceptual models: Advantages, pitfalls and remedies, 41st Workshop on Geothermal Resource Engineering. Stanford University, California, U.S.A (2016a)

Cumming, W.: A conceptual model approach to the geophysical exploration of permeable geothermal reservoirs that considers context and uncertainty. 79th Ann. Internat. Mtg., Soc. of Expl. Geophys. Expanded Abstract (2009b).

Davatzes, N., and Hickman, S.: Fractures, stress and fluid flow prior to stimulation of well (2009), 27-15

Delalande, M.M., Gherardi, F., Williamson, D., Kajula, S., Kraml, M., Noret, A., Abdallah, I., Mwandapile, E., Massault, M., Majule, A., and Bergonzini, L.: Hydrogeochemical features of Lake Ngozi (SW Tanzania). *African Earth* Sciences, **103,** (2015), 153-167.

Delvaux, D., Kraml, M., Sierralta, M., Wittenberg, A., Mayalla, J.W., Kabaka, K., Makene, C., and Geothermal working group: Surface Exploration of a viable geothermal resource in Mbeya area, SW Tanzania. Part I: Geology of the Ngozi-Songwe geothermal system. *World Geothermal Congress, Bali, Indonesia* (2010).

Delvaux, D., Levi, K., Kajara, R. and Sarota, J.: Cenozoic paleostress and kinematic evolution of the Rukwa -North Malawi rift valley (East African rift system). *Bulletin des Centres de Recherches Exploration Production Elfaquitaine* **16,** (1992), 383-406.

Delvaux, D. and Hanon, M.: Neotectonics of the Mbeya area, SW Tanzania. Mus. roy. Afr. centr., Tervuren (Belg.), Dépt. Géol. Min., Rapp. ann. (1993) 1991-1992, 87-97.

Delvaux, D., Kervyn, R., Vittori, E., Kajara, R.S.A., and Kilembe, E.,: Late Quaternary tectonic activity and lake level fluctuation in the Rukwa rift basin, East Africa. *African Earth Sciences,* **26,** (1998), 397-421.

Didas, M.M.: Appendices to the report: "1D joint inversion of MT and TEM data from Ngozi geothermal prospect, southwest Tanzania. An integrated interpretation of geoscientific results". UNU-GTP, Iceland, report 13 appendices, (2018) 96 pp.

East African Rift (EARS): The East African Rift, website, http://www.ics.purdue.edu/~ecalais/projects/ear/tectonics.jpg (2018)

Ebinger, C.J., Deino, A.L., Drake, R.E., and Thesa, A.L.: Chronology of volcanism and rift basin propagation: Rungwe Volcanic Provinces, East Africa. *Geophysical Research*, **94**, (1989) 15.783-15.803.

Ebinger, C.J., Deino A.L., Tesha A.L., Becker, T., and Ring, U.: Regional tectonic controls on Rift Basin Morphology: Evolution of the Northern Malawi (Nyasa) Rift. *J. Geophysical Research*, **98,** (1993) 17.821-17.836.

Eysteinsson, H.: TEMMAP and TEMCROSS plotting programs. ÍSOR – Iceland GeoSurvey, Reykjavík, unpublished programs and manuals, (1998).

Fontijn, K., Delvaux, D., Ernst, G.G.J., Kervyn, M., Mbede, E., and Jacobs, P.: Tectonic control over active volcanism at a range of scales: Case of the Rungwe volcanic province, SW Tanzania; and hazard implications. *J. African Earth Sciences*, **58,** (2010a), 764-777.

Fontijn, K., Ernst, G.G.J., Elburg, M.A., Williamson, D., Abdallah, E., Kwelwa, S., Mbede, E., and Jacobs, P.: Holocene explosive eruption in the Rungwe volcanic province, Tanzania. *J. Volc. Geoth. Res.*, **196,** (2010b) 91-110

Fontijn, K., Williamson, D., Mbede, E. and Ernst, G.G.J.: The Rungwe volcanic province, Tanzania – a review. *J. African Earth Sciences*, **63,** (2012) 12-31.

Garg, S. and Combs, J.: A Reexamination Of USGS Volumetric "Heat In Place" Method, Proceedings, 36th Workshop on Geothermal Reservoir Engineering, Stanford University, Stanford, CA. (2011)

Grant. M.: Resource assessment, a review, with reference to the Australian Code, *Proceedings, World Geothermal Congress, Melbourne, Australia* (2015)

Gibert, E., Bergonzini, L., Massault, M. and Williamson, D.: AMS-14 C chronology of 40.0 cal ka BP continuous deposits from a crater lake (Lake Masoko, Tanzania). *Palaeogeography, palaeoclimatology, Palaeoecology* **187,** (2002), 307-322.

Ingham, M.R., and Hutton, V.R.S.: Crustal and upper mantle electrical structure in southern Scotland: *Geophysics*, **69,** (1982), 579-594.

Jones, A.G.: Magnetotellurics for natural resources: From acquisition through interpretation. Dublin Institute for Advanced Studies (DIAS), (2008), 17–18.

Josephat, S.: Geothermometry and Quantifying of Mixing and water-rock interactions in the Ngozi geothermal field, SW-Tanzania. Report 26 UNU-GTP, Iceland. (2016), 289-310 pp.

Kalberkamp, U., Schaumann, G., Ndonde, P.B., Chiragwile, S.A., Mwano, J.M and GEOTHERM Working Group: Surface exploration of a viable geothermal resource in Mbeya area, SW Tanzania. Part III: Geophysics. *Proceedings of the World Geothermal Congress 2010. Bali, Indonesia*, (2010), 6 pp.

Kraml, M., Schaumann, G., Kalberkamp, U., Stadtler, C., Delvaux, D., Ndonde, P.B., Mnjokava, T.T., Chiragwile, S.A., Mayalla, J.W., Kabaka, K., Mwano, J.M., and Makene, C.: Geothermal Energy as an alternative source of energy for Tanzania. BGR, Germany, GEOTHERM project Technical Cooperation with the Republic of Tanzania, final technical report, (2008), 235 pp.

Marobhe, I.M.: Interpretation of aerogeophysical anomalies of Southwestern Tanzania. Geological Survey of Finland. Bulletin 350. PhD Thesis. (1989), 78 pp.

Meju, M. "Joint inversion of TEM and distorted MT soundings: some effective practical considerations". Geophysics, 61, (1996) 56-65.

Norton Rose Fulbright in Consortium with Omenda, P.: Consultancy Services for preparation of geothermal energy development projects proposal document and M&E system manual for the project. Project proposal document for geothermal resource development. TGDC-September 2017 technical internal report, Unpublished, (2017), 139 pp.

Ochmann, N., and Garofalo, K.: Geothermal Energy as an Alternative Source of Energy for Tanzania, Final Technical Report of Phase II (2010-2013), Technical Cooperation with United Republic of Tanzania, GEOTHERM-Project 2002.2061.6, Unpublished Report, (2013), 156 pp.

Park, S.K., and Livelybrook, D.W.: Quantitative interpretation of rotationally invariant parameters in Magnetotellurics. *Geophysics*, **54,** (1989), 1484-1490.

Phoenix.: Data Processing user guide, SSMT2000, NPIPlot, MTEditor, synchro time series View. Phoenix Geophysics, Ltd, Toronto, Canada (2005).

Pinna, P., France. Bureau de recherches géologiques et minières, Chuo Kikuu cha Dar es Salaam, Geological Survey of Tanzania, BRGM and 20th Colloquium on African Geology.: Geology and mineral map of Tanzania. Orléans, France, (2008).

Ranganayaki, R.P.: An interpretive analysis of magnetotelluric data. *Geophysics*, **49**, (1984), 1730-1748.

TGDC.: Ground truthing survey of the new proposed slim holes locations in Ngozi geothermal prospect. Tanzania Geothermal Development Company, Ltd., internal Technical report, Unpublished (2017), 16 pp.

TGDC.: Geothermal development in Tanzania. Presentation to stakeholders. Dodoma, (2018), 13 pp.

Ussher, G., Harvey, C., Johnstone, R., and Anderson E.: Understanding resistivities observed in Geothermal Systems. *Proceedings World Geothermal Congress 2000, Kyushu-Tohoku, Japan*, (2000)

Wight, D.E.; Bostick, F.X., and Simth, H.W.: Real time Fourier transformation of Magnetoterrulic data; Tech. report, EGRL/EERL, University of Texas, Austin (1977).

Wilmarth, M., and Stimac, J.: Power density in geothermal fields. *Proceedings, World Geothermal Congress, Melbourne, Australia*, (2015), 19-25.

Wight, D.E and Bostick F.X.: Cascade decimation-A technique for real time estimation of power spectrum; (In magnetotelluric methods (ed) Proc. *IEEEIC.ASSP, Soc. Explor. Geophys*, (1980), 626-629